

GRAPHENE BASED NANOCOMPOSITE HYBRID  
ELECTRODES FOR SUPERCAPACITORS

Ashish N. Aphale

Under the Supervision of Dr. Prabir K. Patra

DISSERTATION

SUBMITTED IN PARTIAL FULFILMENT OF THE REQUIRMENTS  
FOR THE DEGREE OF DOCTOR OF PHILOSOHPY IN COMPUTER SCIENCE  
AND ENGINEERING

THE SCHOOL OF ENGINEERING

UNIVERSITY OF BRIDGEPORT

CONNECTICUT

December, 2014

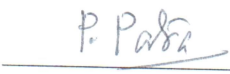

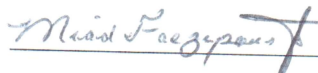
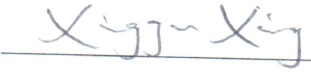
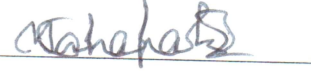
GRAPHENE BASED NANOCOMPOSITE HYBRID  
ELECTRODES FOR SUPERCAPACITORS

© Copyright by Ashish N. Aphale, 2014

# GRAPHENE BASED NANOCOMPOSITE HYBRID ELECTRODES FOR SUPERCAPACITORS

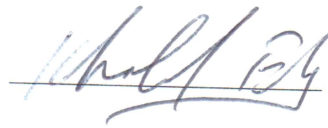
## Approvals

### Committee Members

Name	Signature	Date
Dr. Prabir K. Patra		<u>12-4-2014</u>
Dr. Ausif Mahmood		<u>12-4-2014</u>
Dr. Miad Faezipour		<u>12,04,2014</u>
Dr. Xingguo Xiong		<u>12/04/2014</u>
Dr. Manoj Mahapatra		<u>12/4/2014</u>

### Ph.D. Program Coordinator

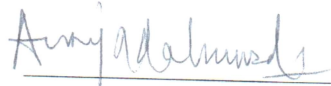
Dr. Khaled M. Elleithy



12/15/2014

### Chairman, Computer Science and Engineering Department

Dr. Ausif Mahmood



12-7-2014

### Dean, School of Engineering

Dr. Tarek M. Sobh



12-16-2014

# GRAPHENE BASED NANOCOMPOSITE HYBRID ELECTRODES FOR SUPERCAPACITORS

## ABSTRACT

There is an unmet need to develop high performance energy storage systems (ESS), capable of storing energy from both renewable and non-renewable sources to meet the current energy crisis and depletion of non-renewable sources. Amongst many available ESS, supercapacitors (ECs) are the most promising because they exhibit a high charge/discharge rate and power density, along with a long cycle life. The possibility of exploring the use of atomically thin carbon allotropes like graphene, carbon nanotubes (CNTs) and electrically conducting polymers (ECPs) such as polypyrrole (PPy) has been studied as a high performance conducting electrodes in supercapacitor application. A novel templated sustainable nanocomposite electrode has been fabricated using cellulose extracted from *Cladophora c. aegagropila* algae as component of the assembled supercapacitor device which later has been transitioned to a unique template-less freestanding nanocomposite supercapacitor electrode. The specific capacitance of polypyrrole-graphene-cellulose nanocomposite as calculated from cyclic voltammetry curve is  $91.5 \text{ F g}^{-1}$  at the scan rate  $50 \text{ m Vs}^{-1}$  in the presence of  $1\text{M NaCl}$  electrolyte. The open circuit voltage of the device with polypyrrole -graphene-cellulose electrode was found to be around  $225 \text{ m V}$  and that of the polypyrrole -cellulose device is only  $53 \text{ m V}$  without the presence of graphene in the nanocomposite electrode. Understanding the

fundamentals by fabricating template nanocomposite electrode, it led to fabricate a unique nanocomposite template-less freestanding film which comprises of polypyrrole-graphene-CNT hybrid. Various experiments have been performed using different electrolytes such ascorbic acid, sodium sulfate and sulfuric acid in different scan rates. The specific capacitance of polypyrrole-graphene-CNT nanocomposite with 0.1 wt% of graphene-CNT, as calculated from cyclic voltammetry curve is  $450 \text{ F g}^{-1}$  at the scan rate  $5 \text{ m V s}^{-1}$ . For the first time a nanofibrous membrane has been developed as a separator which acts as an electrolyte reservoir and ionic diffusion membrane. The performance of the fabricated supercapacitor device has been analyzed using a multimeter and compared with a conventional alkaline (1.5 V) battery. Lighting up of 2.2 V light emitting diode has been demonstrated using the fabricated supercapacitor.

Dedicated to my Family

*To Know the Ignorance is an Intelligence*

## ACKNOWLEDGEMENTS

I would like to express my deepest gratitude to my advisor, Dr. Prabir K. Patra, for his guidance, caring, patience, providing me with an excellent atmosphere and connecting me to top experts in the field for doing research. It is my honor to be one of his first Ph.D. students. Besides my advisor I would like to thank the rest of my thesis committee: Professor Ausif Mahmood, Professor Miad Faezipour, Professor Xingguo Xiong and Dr. Manoj Mahapatra for their encouragement, insightful comments and support.

My sincere thanks to Professor Angela Santiago in the Department of Chemistry at University of Bridgeport, whose expertise and experience in the field of electrochemistry has helped my thesis a lot. I thank Dr. David Burton for his support as well.

I am fortunate to have been associated with and have learned from Professor Prabhakar Singh and Dr. Manoj Mahapatra at Center for Clean Energy Engineering (C2E2), University of Connecticut. Their expertise and continuous advice helped me to shape my thesis with great confidence. I am fortunate and very grateful that they provided me full access to their state-of-the-art lab which led to this quality work.

Many thanks, to my colleague and a longtime friend Dr. Isaac Macwan for his deep discussion on the topics and designing experiments. I wish him and his family



success in future. I would also like to thank Bhushan Dharmadhikari for his help in discussing experimental work towards my thesis work. I thank to Ms. Krushangi Maisuria, Ms. Roquie Wie (Vinnie), Mr. Shrinivas Bhosale (Shrini) and Mr. Kapil Mahakalkar (Kaps) whom I worked with in lab and did a lots of experiments and discussions and fun. My research would not have been possible without their help.

I would like to thank University of Bridgeport for providing SEED money grant scholarships on, “Functional Proteins for DNA Mismatch Repair: A Novel Nano-biosensor for Cancer Diagnostics” and “DNA-graphene based piezoelectric device”.

Above all, I want to thank my mother and father for their love and encouragement in everything I have ever strived for and teaching me to never give up. It is because of their hard work, patience, love and infinite sacrifices that I was able to make my dream come true. I would like to thank my father from whom I learnt a great deal of fundamental science and creative experimental suggestions which helped in actualizing my hypothesis. I would also like to thank my two elder sisters and their family for cheering me up in everything I did and encouraging me with their best wishes.

During this wonderful journey, there were many individuals I came across, many of them for short period of time and there were few associated for long period of time. I would like to thank everybody whom knowingly or unknowingly, willingly or unwillingly has influenced me in a right way and have motivated me to keep pursuing my dreams. I would personally like to thank all of them and I will be obliged to them.

# TABLE OF CONTENTS

ABSTRACT .....	iv
ACKNOWLEDGEMENTS .....	viii
TABLE OF CONTENTS .....	x
LIST OF TABLES .....	xv
LIST OF FIGURES .....	xvii
CHAPTER 1. INTRODUCTION .....	25
1.1 Research Problem and Scope .....	25
1.2 Motivation behind the Research .....	28
1.3 Potential Contributions of the Proposed Research .....	30
1.4 Energy Storage Systems.....	31
1.4.1 Conventional Capacitors .....	32
1.4.2 Batteries .....	34
1.5 Introduction to Supercapacitors.....	35
1.5.1 Working principle of supercapacitors.....	37
1.5.2 Double Layer Capacitor.....	37

1.5.3 Pseudocapacitors .....	39
CHAPTER 2.    MATERIALS FOR ELECTRODE.....	41
2.1 Graphene .....	41
2.2 Carbon Nanotubes.....	44
2.3 High Surface Area Active Materials .....	45
2.4 Carbon based Nanocomposite .....	47
2.5 Cellulose as Substrate .....	49
2.6 Electrolytes.....	50
CHAPTER 3.    GOALS OF RESEARCH.....	51
CHAPTER 4.    SYNTHESIS AND ELECTROCHEMICAL ANALYSIS OF ALGAE CELLULOSE-POLYPYRROLE-GRAPHENE NANOCOMPOSITE FOR SUPERCAPACITOR ELECTRODE .....	52
4.1 Electrode Fabrication .....	52
4.1.1 Cellulose Extraction.....	52
4.1.2 Graphene synthesis and processing .....	53
4.1.3 Polymerization of Pyrrole .....	54
4.1.4 Nanocomposite Paper Fabrication.....	56
4.1.5 Supercapacitor Device Assembly.....	56
4.2 Characterization Techniques .....	57

4.2.1	Scanning Electron Microscopy (SEM) .....	57
4.2.2	Transmission Electron microscopy (TEM) .....	60
4.2.3	Atomic Force Microscopy (AFM) .....	65
4.2.4	UV-Resonance Raman Spectroscopy (UVRR) .....	65
4.3	Electrochemical Analysis of the electrode .....	66
CHAPTER 5. A NOVEL TEMPLATE-LESS HYBRID NANOCOMPOSITE		
ELECTRODE FOR SUPERCAPACITOR.....		
5.1	Nanocomposite electrode fabrication .....	70
5.2	Materials and methods .....	70
5.2.1	Pyrrole solution: .....	70
5.2.2	Pyrrole-graphene-CNT (PCG) solution: .....	70
5.2.3	Graphene and carbon nanotube: .....	71
5.2.4	Polymerization of Pyrrole and nanocomposite solutions.....	72
5.2.5	Fabrication of Freestanding Nanocomposite Film .....	73
5.2.6	Electrolyte comparison .....	75
5.3	Scanning electron microscopy.....	75
5.3.1	Polypyrrole.....	75
5.3.2	Cross section of Polypyrrole films .....	76

5.3.3 Scanning electron microscopy of Polypyrrole after 100 cycles of cyclic voltammetry in sodium sulfate electrolyte .....	77
5.3.4 Scanning electron microscopy of Polypyrrole-graphene-CNT nanocomposite electrode after 100 cycles of cyclic voltammetry in sodium sulfate electrolyte .....	78
5.3.5 Polypyrrole-graphene nanocomposite electrode (PG).....	79
5.3.6 Polypyrrole-graphene-CNT nanocomposite electrode (PCG) .....	80
5.4 Energy- dispersive X-ray spectroscopy (EDS).....	81
5.5 Electrochemical Analysis of the nanocomposite electrodes in different electrolytes .....	82
5.6 Power density and Energy density comparison of the electrodes .....	89
CHAPTER 6. SUPERCAPACITOR DEVICE ASSEMBLY .....	91
6.1 Fabrication of PCL based nanofibrous separator membrane .....	92
6.1.1 Model for formation of aligned nanofibers on the rotating collector .	93
6.1.2 Finite Element based simulation model.....	97
6.2 Electrical measurements of the supercapacitor device .....	99
6.2.1 Circuit Implementation .....	101
CHAPTER 7. APPLICATION SPECIFIC MODELING OF THE SUPERCAPACITOR .....	104

7.1	Mathematical model for theoretical specific capacitance of the polypyrrole electrode in sulfuric acid.....	104
7.1.1	Estimate of maximum value of specific capacitance.....	105
7.2	Supercapacitor in hybrid electric vehicles (HEV) application .....	107
7.3	Mathematical model for power backup using supercapacitors to prevent data loss .....	108
7.3.1	Backup power application.....	109
7.4	Microelectrode supercapacitor .....	111
	CONCLUSIONS .....	112
	REFERENCES .....	114

## LIST OF TABLES

Table 5-1	Cyclic voltammetry parameters for depositing pyrrole and pyrrole-CNT-graphene nanocomposite free standing films	72
Table 5-2	List of the different nanocomposite supercapacitor electrodes with varying concentration of graphene and CNT in the overall pyrrole matrix.	82
Table 5-3	Weight of individually deposited nanocomposite freestanding film for electrochemical analysis.	83
Table 5-4	Specific capacitance values of individual nanocomposite films in sulfuric acid (SA) electrolyte as measured by cyclic voltammetry.	85
Table 5-5	Specific capacitance values of individual nanocomposite films in sodium sulfate (SS) electrolyte as measured by cyclic voltammetry.	85
Table 5-6	Specific capacitance values of individual nanocomposite films in ascorbic acid (AA) electrolyte as measured by cyclic voltammetry.	86

Table 6-1	Test cases for the implemented circuit	102
Table 7-1	Technical data, Toyota Prius, 2008	107



## LIST OF FIGURES

Figure 1-1	Ragone type plot summarizing the specific power density of various energy storage devices as a function of their specific energy density. Reprinted by permission from Macmillan Publishers Ltd: Nature Materials, [1], copyright (2008).	26
Figure 1-2	Greenhouse Gas Emissions only in U.S	28
Figure 1-3	Transistor showing low working voltage and high current output. "Reprinted with permission from [35]. Copyright [2005], AIP Publishing LLC.	29
Figure 1-4	Schematic of conventional capacitor with dielectric sandwiched between two conductive plates	32
Figure 1-5	Working principle of Lithium-Ion battery	35
Figure 1-6	Schematic representation of electric double layer supercapacitor	36
Figure 1-7	Simplified electric circuit representation of supercapacitor [46]. Reprinted from [46], Copyright (2006), with permission from Elsevier	38

Figure 2-1	Schematic illustration of various forms of carbon allotropes. Adapted from [21]. Reprinted by permission from Macmillan Publishers Ltd: Nature Materials[59], copyright (2007)	42
Figure 2-2	Visual transparency of graphene [67]. Reprinted with permission from AAAS	43
Figure 2-3	Transmission electron microscope image of multi walled nanotubes comprised of an array of several single walled nanotubes. Image adopted from [68], Nature publishing group, copyright 1992	44
Figure 2-4	a) TEM image of onion-like carbon. Reprinted from [85] Copyright (2007), with permission from Elsevier, b) SEM of array of CNT on SiC. Reprinted from [127], copyright (2008), with permission from Elsevier	46
Figure 2-5	An overview of various carbon based nanocomposite supercapacitors of different structures and forms. Reproduced from [98] with permission of The Royal Society of Chemistry	48
Figure 4-1	A) Optical image of algae ball prior to cellulose extraction, B) Algae cellulose extracted in pulp form after the hydrolysis, C) Filtered cellulose pulp	53
Figure 4-2	Graphene oxide solution after sonication for 2hr.	53

Figure 4-3	A) Solution preparation of Py and Tween80 with varying concentration of graphene, B) Cellulose pulp addition to Py solution containing Tween80 and graphene	55
Figure 4-4	Optical images of various stages of conductive paper fabrication. Image (A,B) Cellulose coated with PPy and graphene being given a rectangular shape by applying pressure in order to get desired thickness. Image (C, D) Final conductive paper electrode without and with graphene respectively	56
Figure 4-5	Picture of supercapacitor device made from conducting nanocomposite electrodes.[110]	57
Figure 4-6	SEM micrograph of graphene oxide with the concentration of 0.16mg/ml at magnification of x5000, revealing a typical platelet like structure. [111]	58
Figure 4-7	SEM micrograph of graphene nanoplateletes dispersed in 7X Tris-EDTA buffer [111]	59
Figure 4-8	SEM micrograph of nanocomposite with cellulose fibers coated with no graphene (A-C) and with 0.01 wt% graphene (D-F)[110]	60
Figure 4-9	TEM micrograph of graphene oxide dispersed in water by sonication.	61
Figure 4-10	Proposed hydrogen bonding network formed between	62

	oxygen functionality on GO and water. Reproduced from [112] with permission of The Royal Society of Chemistry (RSC)	
Figure 4-11	TEM micrograph of graphene dispersion in 7X TE buffer.	63
Figure 4-12	TEM micrograph of cellulose-PPy-graphene nanocomposite, (A,B) cellulose-PPy, (C,D) cellulose-PPy-graphene (0.005g) [110]	64
Figure 4-13	Tapping mode AFM image of graphene oxide deposited on a freshly cleaved mica surface with height of ~0.9nm [115]	65
Figure 4-14	UV-Raman spectra of graphene dispersed in 7x TE buffer [111]	66
Figure 4-15	Cyclic voltammetry curves obtained using A) PPy-cellulose, B) PPy-graphene-cellulose nanocomposite at scan rate of 50mVs <sup>-1</sup> in aqueous 1M NaCl electrolyte. [110]	67
Figure 4-16	Variation of specific capacitance of PPy-cellulose and PPy-graphene-cellulose nanocomposite as a function of scan rate. (Inset: Specific capacitance change as function of graphene concentration at scan rate of 50 mVs <sup>-1</sup> )[110]	68
Figure 4-17	Supercapacitor reading using multimeter recorded over 4 days. [110]	69
Figure 5-1	Polymerization of pyrrole using three electrode setup CV	73

	with Pt (WE), graphite rod (CE) and Ag/ AgCl (RE)	
Figure 5-2	Polymerization of pyrrole (Py) to conductive polymeric chain of polypyrrole (PPy)	73
Figure 5-3	Optical images of PPy film formation on graphite substrate. A free standing film can be peeled off to be used as an electrode. A) Control PPy film, B & C) PPy-graphene-CNT film.	74
Figure 5-4	SEM micrographs of control PPy electrodes at various magnifications	76
Figure 5-5	Cross- sectional SEM micrographs of PPy	77
Figure 5-6	Needle like structures seen in the SEM micrograph of the controlled PPy film after performing cyclic voltammetry in 1M Na <sub>2</sub> SO <sub>4</sub> (SS) electrolyte, suggesting the degradation of the polymer film over the time	78
Figure 5-7	SEM images of post CV done for 100 cycles to observe the degradation in the samples of PCG0.01	79
Figure 5-8	High resolution SEM micrograph of PPy-graphene (PG 0.1 wt %) concentration at different magnification showing a very unique nanocomposite structure	80
Figure 5-9	SEM micrograph of polypyrrole-graphene-CNT nanocomposite electrode film.	81
Figure 5-10	Elemental EDS characterization representing the	81

	composition of control PPy film before performing the CV	
Figure 5-11	Cyclic voltammetry comparison of the control PPy nanocomposite in various electrolytes (SA, SS, AA). A typical capacitive curve is obtained by the PPy nanocomposite in SA electrolytes representing higher charge storing capability	84
Figure 5-12	Specific capacitance verses the scan rate. Overall observation of higher specific capacitance in SA followed by the SS and least in AA.	87
Figure 5-13	Specific capacitance measurements of individual electrodes such as control PPy and different concentrations of PCGs in various electrolytes (SA, SS and AA)	88
Figure 5-14	A superimposed graph of PCG containing nanocomposite at various scan rates on a Ragone plot which compares the electrodes of supercapacitors from various reference and commercially available supercapacitors. Reproduced from [120], Scientific reports, 2013	89
Figure 6-1	Supercapacitor test assembly cell device. Left image adapted from [121], image on the right is of the actual supercapacitor device.	91
Figure 6-2	A) Typical electrospinning setup having high voltage power supply and syringe pump, B) SEM image of the	92

PCL nanofibers showing nanofibrous structure with average diameter in the range of 600 nm, C) SEM image of electrospun nanofibers completely oriented in one direction using rotating collector

- Figure 6-3 Schematic showing various forces acting on a polymer drop at the tip of needle leading to subsequent stretching 93
- Figure 6-4 Electric Field modeling and analysis showing the electric field pattern at the collector surface. (a) Distance between the needle (positive terminal) and the collector (ground) showing the electric field lines. The length and thickness of the arrows is proportional to the intensity of the field (maximum of 122.7 V/m), (b) a 3-D view of the model showing the electric field predominantly over the periphery of the disc collector anticipating a larger accumulation of nanofibers over the periphery, (c) line graph plot showing the highest intensity of the electric field at the periphery of the 30cm diameter collector. The difference in field strength ( $\sim 1000\text{V/m}$ ) between the two edges is due to the error in positioning the arc across the disc collector 98
- Figure 6-5 A) Supercapacitor device assembled and ready to be tested. 99  
B) Measurement of the output voltage from a conventional

alkaline 1.5 V battery, C) Output voltage of supercapacitors stacked in three cells made from CR2032 stainless steel coins. The overall output voltage of the device is approximately 1.5 V

- Figure 6-6      Charging of the supercapacitor device using external power supply with constant 5V / 3A. The supercapacitor device needs to be charged only for 10 s giving the output voltage of ~2.5 V. B & C) Demonstrates the lighting up of green LED (2.2V) using the supercapacitor device after charging      100
- Figure 6-7      A) Experimental circuit implementation for demonstration of supercapacitor performance, B) Circuit diagram illustrating the same circuit design      101
- Figure 6-8      Comparison of a conventional capacitor with stacks of supercapacitor using the implemented circuit.      103
- Figure 6-9      Discharge profile of the supercapacitor stack with and without the presence of load (LED) with respect to time (min)      103
- Figure 7-1      Photograph of a capacitive microelectrode demonstrating the capability of precisely depositing electrically conductive electrode with higher performance.      111



# **CHAPTER 1. INTRODUCTION**

## **1.1 Research Problem and Scope**

Global warming and depleting fossil fuels have forced us to move towards sustainable and renewable resources for energy production. Along with the development of electric vehicles or hybrid electric vehicles which produce low greenhouse gas emissions, we are witnessing increasing innovations towards renewable sources of energy production like solar and wind as well. As these renewable resources of energy are not available on demand, energy storage systems are starting to play an important role in our lives. Currently the most popular commercialized energy storage devices are batteries, capacitors and fuel cells. However, because of our ever increasing appetite for energy, there is a need to improve the performances of these devices to satisfy high power requirements of various systems ranging from portable electronics to hybrid vehicles and large industrial equipments. The gap between the performances of devices and the power requirement can be filled by discovering new materials for energy storage and advancing our understanding of the electrochemical interfaces at the nanoscale level.

Great efforts have been made on research and development of high performance energy storage devices in the past; however, the slow power capability and high maintenance cost have kept them away from many applications. Recently, supercapacitors have drawn much attention because of their high charge/discharge rate,

long life cycle and outstanding power density[3]–[6]. Supercapacitors, also known as ultracapacitors or electrochemical capacitors (ECs), store energy using either ion adsorption electrochemical double layer capacitors (EDLC) as electrical charge on highly porous materials or surface redox reactions (pseudo-capacitors). The key in achieving high charge storage capabilities in supercapacitors is attributed to high SSA in electrode materials where it can store hundreds or thousands of times more charges than electrodes in batteries or capacitors as shown in Figure 1-1.

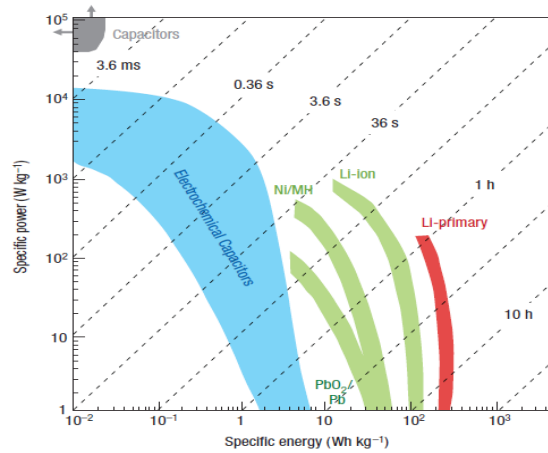


Figure 1-1 Ragone type plot summarizing the specific power density of various energy storage devices as a function of their specific energy density. Reprinted by permission from Macmillan Publishers Ltd: Nature Materials, [1], copyright (2008).

It is very important to assess the capabilities of these energy storage devices in terms of energy density and power density based on their unit mass or volume. Ragone plot[1] (Energy density v/s Power density) is a comparative chart used for performance comparison of different energy storage devices. As seen from (Figure 1-1above) capacitors are in the extreme end of the chart having very high specific power ( $\text{W kg}^{-1}$ ) but are extremely low on the specific energy ( $\text{W h kg}^{-1}$ ). On the contrary, batteries

possess very high specific energy but extremely low specific power. In comparison to batteries and conventional capacitors, supercapacitors have at the same time higher specific energy as well as higher specific power[7]. In other words if an electric vehicle runs on supercapacitors, the specific power shows how fast one can go and specific energy shows how far one can go on a single charge[1].

Graphitic carbons are one of the several materials which have very high SSA and open porosity which gives high capacitance[2]. Besides activated carbons, carbide-derived carbons[8], carbon fabrics[9], nanotubes[10], onions[11], and nanohorns[12] have been used in supercapacitors. Several electrically conductive polymers (ECPs) are used as pseudocapacitive supercapacitors like polypyrrole (PPy)[13], [14], polyaniline (PANI)[15], [16], polyindoles, etc[17], [18]. One promising electrode material candidate for EDLC is graphene[19] due to its unique lattice structure, exhibits appealing electrical properties, chemical stability and high surface area[20]–[22].

The key challenge in making better performance supercapacitors based energy storage device is to develop nanocomposite material based electrode with high enough SSA where the ionic adsorption takes place very fast and more energy can be stored in the device. A combination of pseudocapacitive materials such as electrically conductive polymers (ECPs) and high SSA materials like graphene and CNTs can be a unique nanocomposite used as an electrode for supercapacitor. Another challenge in fabricating electrode for supercapacitors is to make a free standing film made from these nanocomposites. Natural materials such as coconut shells, cotton or other textile based fabrics and cellulose based papers can be good choice as a substrate material for making

free standing film[1]. Fabricating a very safe and environmentally sustainable “green” supercapacitor based on abundant or renewable materials which are non toxic is thus a key challenge and necessity.

## 1.2 Motivation behind the Research

Human activity and energy supplies mainly rely on the consumption of non-renewable fossil fuels. According to Institute for Energy Research (IER) 80 % of the total energy produced only in US is dependent on fossil fuels like coal, natural gas and petroleum. According to U.S. Energy Information Administration the world energy consumption will increase from 524 quadrillion Btu in 2010 to 630 quadrillion Btu in 2020. According to U.S. Greenhouse Gas Emissions and Sinks (Figure 1-2), about 28% of the total green house gas only in the U.S is emitted by transportation and 32% from the electricity generation[23].

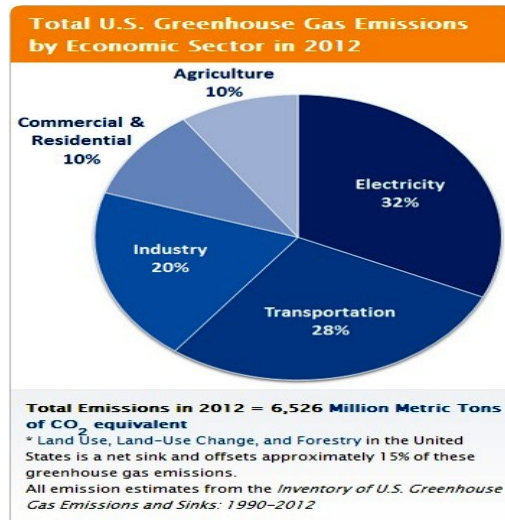


Figure 1-2: Greenhouse Gas Emissions only in U.S

Therefore, there is an urgent need to develop energy storage technologies to combat global warming and climate change[24], [25]. Extensive research has been performed on the development of solar cells[26], [27], fuel cells[28], lithium-ion batteries[29], [30] and supercapacitors[31], [32] to replace fossil fuel-based energy sources. Both portable consumer electronics as well as electric vehicles are strongly dependent on the storage of electrical energy and thus, the need and importance of electric storage systems is increasing strongly[5], [33], [34]. Beside this more and more energy production units are encouraged from the renewable sources of energies. However, these sources of energies are not available on demand as we may not get energy from sun in certain time of the day or certain period of year wind energy is not enough that is where a need to develop high performance energy storage systems is essential.

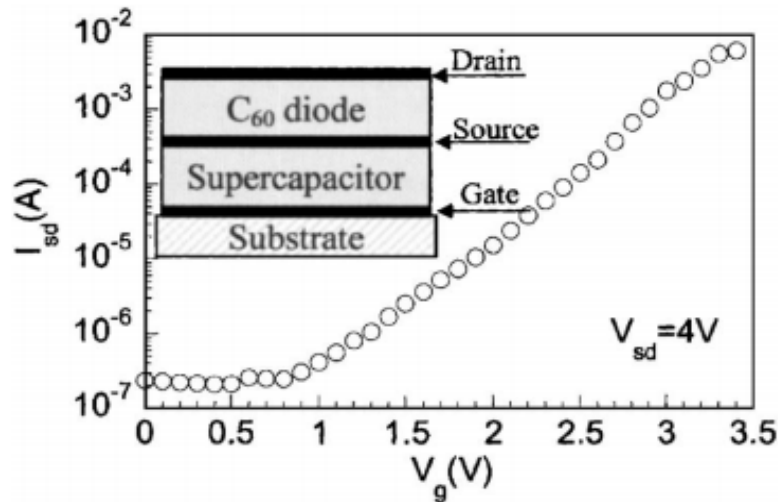


Figure 1-3: Transistor showing low working voltage and high current output. "Reprinted with permission from [35]. Copyright [2005], AIP Publishing LLC.

Supercapacitors have also started to play very important role in the area of Very Large Scale Integration (VLSI). Supercapacitors can also be used in memory backup systems which can provide power during failure of primary power sources. Supercapacitors can be also be used as a building block in electronic devices such as organic diodes and organic memory devices[36]–[39]. Ma and coworkers[40] has shown this previously by inserting a supercapacitor in an organic diode.

### **1.3 Potential Contributions of the Proposed Research**

- 1) A fundamental understanding of nanocomposite material and their nanostructure morphology will be a key contribution in the field of energy storage in general and supercapacitor in particular.
- 2) A method to fabricate “green” electrode made from organic materials a substrate such as cellulose extracted from marine algae and coating it with conducting polymer and graphene is addressed.
- 3) Fabrication method to produce free standing films made from polypyrrole-graphene -CNT as an electrode is addressed.
- 4) Electrochemical analysis of these materials and the supercapacitor device fabrication protocol is developed and the device performance has been compared with the existing commercial technologies such as alkaline batteries and conventional capacitors.
- 5) A novel use of nanostructured polycaprolactone (PCL) based separator membrane with extremely small diameters of the nanofibers in the range of 100-500 nm.

This separator membrane has been fabricated using electrospinning process enabling very low resistance for the ionic diffusion across the electrodes.

In general, an improved understanding of charge storage mechanism in electrode material pores will help to expand our fundamental understanding toward improved energy storage performances. Flexible, printable and wearable energy storage devices are likely to be integrated into smart clothing, sensors, and wearable electronics and drug delivery systems. In some instances they will replace batteries, but in many cases they will either complement batteries, increasing their efficiency and lifetime, or serve as energy solutions where an extremely large number of cycles, long lifetime and fast power delivery are required.

#### **1.4 Energy Storage Systems**

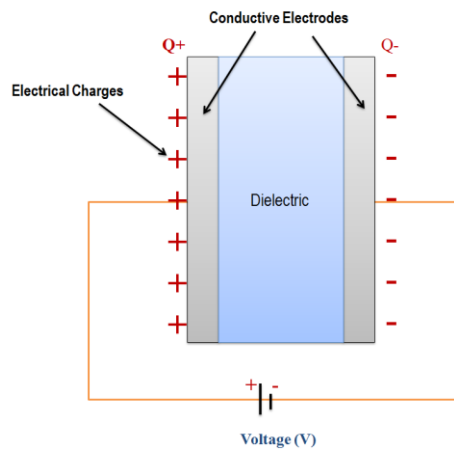
The worldwide appetite for energy grows while diminishing non renewable sources of energy and the threat posed by negative environmental consequences of their use is no longer in questions[41] . Observations of increased levels of CO<sub>2</sub> in the earth's atmosphere and a correlated rise in global temperature have motivated the efforts to reduce or eliminate the dependency on fossil fuels to fulfill future energy demands. Total world consumption of energy will continue to increase, motivating the need to investigate alternative means of energy production, use and storage.

There are increasing efforts seen in production of energy from renewable sources like wind and sun to meet the ever increasing energy demands. Although the renewable resources are practically infinite, their continuous availability is not. In the night or when cloudy we may not derive solar power or during certain time of year we may not get wind

power to produce enough energy to meet the required energy demand. One of the distinctive characteristics of the electric power sector is that demand for electricity fluctuates throughout the day. Currently there are three major commercialized energy storage devices are capacitors, batteries and fuel cells. To illustrate the advantage of supercapacitors, the structure, mechanism and performance comparison of those devices are discussed in the following sections

### 1.4.1 Conventional Capacitors

A conventional capacitor also known as electrostatic capacitor as shown in stores the charges by the virtue of electrostatically between two conducting plates. These conducting plates also called electrode are separated by a dielectric layer (insulator) as shown in *Figure 1-4*.



*Figure 1-4:* Schematic of conventional capacitor with dielectric sandwiched between two conductive plates.

When the external voltage is applied across two electrodes the charges from the dielectric medium gets separated, where anions (-ve ions) will get attracted to



positively charged electrode, and cations (+ve ions) thus generating an electric field which allows the device to store energy. Capacitors generally can release the stored charge quite fast resulting in a high power, but cannot store much energy.

The characteristic parameter for a capacitor is capacitance  $C$  is the ratio of  $Q$  to  $V$

$$C = \frac{Q}{V} \quad (1.1)$$

Here the  $C$  is capacitance,  $Q$  is the charge and  $V$  is the applied external field.

For a capacitor consisting of two parallel plates with surface area of  $A$  separated by a dielectric with permittivity of  $\epsilon$  and a thickness of  $d$ , the voltage is defined as shown in (1.2)

$$V = - \int_0^d \zeta dx = \iint_0^d \frac{\rho}{\epsilon} dx = \int_0^d \frac{Q}{\epsilon A} dx = \frac{Qd}{A} \quad (1.2)$$

Hence in general the capacitance would be as :

$$C = \frac{\epsilon A}{d} \text{ or } C \propto \frac{1}{\text{thickness}} \quad (1.3)$$

As seen above in (1.3), the capacitance is inversely proportional to the thickness of the dielectric medium. Typical thickness in a conventional capacitor can be somewhere near 1000 nm. The effort to decrease the thickness of dielectric medium in a conventional capacitor using advanced fabrication methods will increase the overall cost of the capacitor substantially.

ESDs are typically characterized based on their specific energy and specific power (per unit mass)

Hence energy  $E$  stored in a capacitor is:

$$E = \frac{1}{2} CV^2 \quad (1.4)$$

And the power is derived over time  $\delta t$  required to discharge the capacitor:

$$P = \frac{\partial E}{\partial t} \quad (1.5)$$

As seen from Ragone's plot (*Figure 1-1*) on an average a capacitor can have a power density of  $10^5 \text{ W kg}^{-1}$  and energy density of  $10^{-2} \text{ E h kg}^{-1}$ . It can be seen that conventional electrostatic capacitors can deliver large amount of power, they can be charged/ discharged very quickly in an average 3.6 m s, but they can store less amount of energy.

### 1.4.2 Batteries

A battery is an energy storage device that uses a redox reaction to convert the stored chemical energy into electrical energy. Electrochemical cell in a battery consists of two electrodes which are connected to a conductive electrolyte. Batteries in general are powered by a redox reaction with a reduction of cation at the cathode and oxidation of anions at the anode. If we consider a rechargeable lithium ion battery as shown in *Figure 1-5*, it consists of graphite as a negative electrode (anode) and  $\text{LiCoO}_2$  as cathode with a non-aqueous electrolyte.

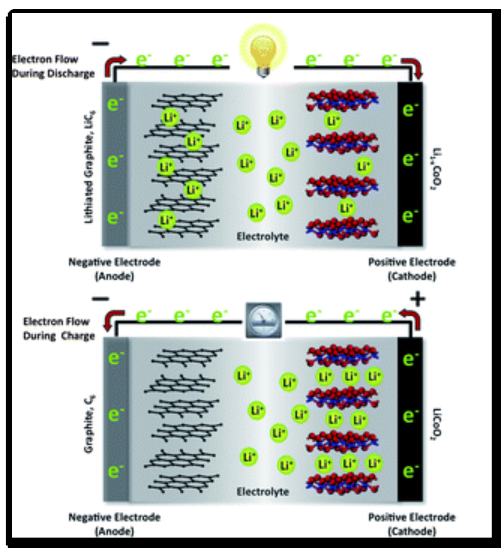


Figure 1-5: Working principle of Lithium-Ion battery

While charging, Li ions are deintercalated from layered  $\text{LiCoO}_2$  at the cathode and diffusing through the electrolyte is intercalated to graphite between the layers at the anode. On discharging, the process reverses with lithium-ions transporting from the anode to the cathode. In batteries the whole material participates in the process of energy transfer and hence a bulk amount of energy can be stored. Hence the energy density of batteries is very high but their power density is low. In general, batteries have energy density  $10^2 \text{ W h Kg}^{-1}$  and power density in the regime of  $10^3 \text{ W Kg}^{-1}$ .

## 1.5 Introduction to Supercapacitors

Supercapacitors are energy storage devices as shown in *Figure 1-6*; having two conducting electrodes separated by a dielectric membrane which is soaked with electrolyte solution.

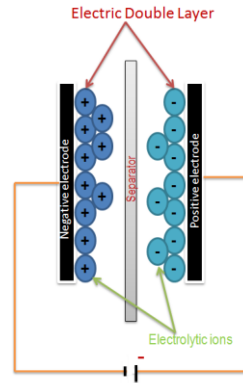


Figure 1-6: Schematic representation of electric double layer supercapacitor

This dielectric membrane allows the passage of ions through. Under the influence of an external electric field, the ions from the electrolyte get separated and the opposite ions get attracted to the respective electrode. Ions will transfer through the dielectric membrane and they will get adsorbed on the surface of the electrode pores creating a layer of the ions on the surface. This layer is called electric double layer and the thickness of this layer is the effective thickness to produce required capacitance and the energy storage (refer (1.3)). Generally, with the aqueous electrolytic ions on the electrode surface the thickness can be achieved in the range of few nm or in Å scale[8], [42]. The overall specific capacitance can be in the order of few hundreds of  $F g^{-1}$ .

The fabrication of electrode and design of its composite structure is very important in order for these ions to access higher specific surface area improving overall energy storage. In addition to that, a low equivalent series resistance (ESR) value can help maintain a very high power density. The charge storing mechanism in supercapacitors unlike batteries does not undergo any chemical or phase change, which

makes it highly reversible and can be repeated for a large number of charge-discharge cycles[1].

### **1.5.1 Working principle of supercapacitors**

Supercapacitors also known as ultracapacitors, electrochemical capacitors or hybrid capacitors were first recognized General Electric in 1957. The finding was patented by Becker, were they found out that this capacitor can store a high capacitance by a double layer mechanism[43]. Later in 1972 Nippon Electric Company (NEC, Japan) first commercialized the supercapacitor in an aqueous electrolyte[44]. Since 2000, supercapacitors have effectively been used in various industrial applications such as automobiles, tramways, buses, electrical load leveling in stationary and transport systems, etc[45]. A recent example of a reported use of supercapacitors was in the emergency doors on an Airbus A380[1]. Supercapacitors have higher energy density (average 5 Wh kg<sup>-1</sup>) than the conventional capacitors. Supercapacitors consists two electrodes and suitable electrolyte packed all together in a very small assembly for by ion adsorption (electrochemical double layer capacitance) or fast surface redox reactions (pseudocapacitance).

### **1.5.2 Double Layer Capacitor**

A very high SSA porous electrode is attached to the current collector on either side sandwiching the separator soaked with electrolyte. Upon the application of voltage potential across the electrodes the electrons will accumulate at the surface of negatively charged electrode, creating holes at the same time on positively charged electrode.

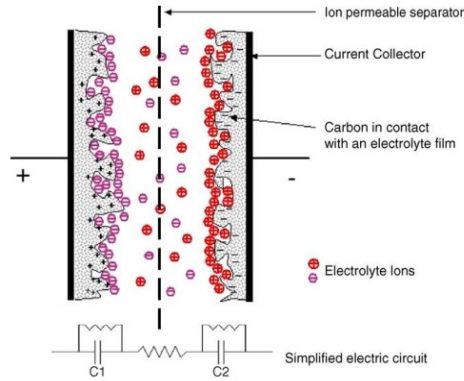


Figure 1-7: Simplified electric circuit representation of supercapacitor [46]. Reprinted from [46], Copyright (2006), with permission from Elsevier.

To balance the charge neutrality, anions and cations are exchanged across the separator on each side hence creating a layer at the surface of both the electrodes known as electric double layer (EDL). The thickness of this layer is usually in the order of few nanometers (nm), dependent on the radius of a solvated ion. The capacitance produced in a supercapacitor is dependent on the effective thickness of this double layer. Hence the nm scale charge separation and very high SSA electrode surface leads in achieving significantly high capacitance.

As shown in Figure 1-7 here the EDLC based supercapacitor utilizes two parallel plates having individual capacitance. The total measured capacitance of the system would be

$$\frac{1}{C_{cell}} = \frac{1}{C1} + \frac{1}{C2} \quad (1.6)$$

In EDLCs a strong interaction happens between the ions in the electrolyte and electrode surface. The solvated ions adsorbed on electrode surface have long term

electrostatic interactions but not any kind of chemical reactions. The double layer can be controlled by various factors such as composition of electrolytes and structural morphological design of the electrode surface.

### 1.5.3 Pseudocapacitors

Pseudocapacitors are faradaic in nature in contrast to electrostatic capacitors having double layer and they take advantage of redox reactions at the surface of the electrode, creating the capacitance. Much similar to batteries, pseudocapacitance is caused by the oxidation state changes of the electrode material during the interactions of ions in the electrolyte with the surface of the active materials[1]. The capacitance of pseudocapacitive based electrode can be calculated using following equation[47]

$$C = \frac{(\Delta q)}{(\Delta V)} \quad (1.7)$$

Here,  $\Delta q$  is the charge transferred and  $\Delta V$  is the electrode potential

Conducting polymers such as polyaniline (PANI) and polypyrrole (PPy) have been utilized previously as supercapacitor electrode with pseudocapacitive behaviors[1], [15], [48]. The reported specific capacitance of pure PANI electrodes [49] ranges in 160 to 800 F g<sup>-1</sup>. Pure PPy exhibits specific capacitance values of 480 F g<sup>-1</sup> in non-aqueous systems[50]. The effect of pseudocapacitance as fast redox reactions can also be exploited using oxygen- or nitrogen containing surface functionalities[51], [52], utilizing redox-active electrolyte[53] at the electrode material surface such as iodide or iodine[54]. They have less dependency on the surface area and shown to deliver higher specific

capacitance than EDLC mechanism[2]. However a major drawback of surface reactions on the electrode is they cause degradations of material eventually causing failure and reducing cycling stability.



## **CHAPTER 2. MATERIALS FOR ELECTRODE**

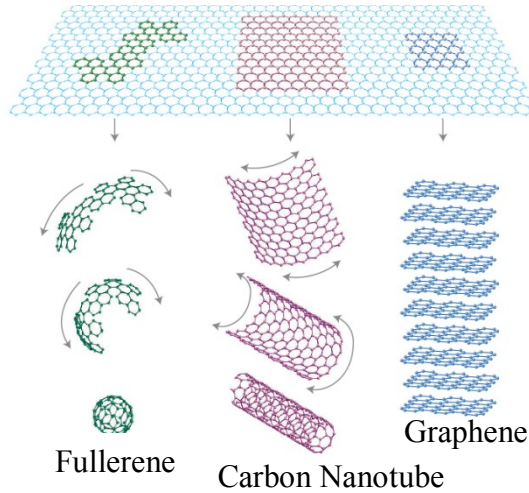
The key in achieving high performance of the electrode for energy storage is the use of materials exhibiting high specific surface area, high conductivity and better stability. Amongst many materials available graphitic carbons and electrically conducting polymers (ECPs) are one the best choice to fabricate the electrodes for supercapacitors.

### **2.1 Graphene**

The name graphene was derived from a Greek word, “graphein” meaning to write[55]. Graphene is a primary building block of graphite which has a lamellar structure with unique electronic and mechanical properties. Individual layers of these lamellar structure are stacked together by van der Waals forces and are considered to be independent entities[56]. It was predicted using a series of theoretical analysis that these layers- if peeled off- might exhibit extraordinary electronic properties[56]. These prediction were proven after almost 60 years, when the individual layers of graphite were separated and their mechanical and electrical properties were tested[20], [21], [57], [58]. In nutshell, each layers of carbon atom that is isolated from the matrix of graphite is known as “graphene”.

There are various routes to synthesize graphene using the starting materials like graphite oxide (GO), graphene oxide (exfoliated GO) and graphite intercalated

compounds (GICs)[60]–[62]. Reduce graphene oxide (r-GO), a very similar material to pristine graphene is prepared by chemical modification of GO and graphene oxide[63], [64].



*Figure 2-1:* Schematic illustration of various forms of carbon allotropes. Adapted from [21]. Reprinted by permission from Macmillan Publishers Ltd: Nature Materials[59], copyright (2007).

In an effort by Schafhaeutl by using strong acids such as sulfuric and nitric, as well as oxidants such as  $\text{KClO}_3$  on graphite, resulted in the intercalation of the layers of graphite, chemical oxidation of its surface leading to the formation of GO[65], [66]. The functionalization of the surface of graphite using chemical modifications lessens the interplanar forces that cause lamellar stacking. These layers once oxidized now can be readily exfoliated under ultrasonic, thermal or other mechanisms.

Geim, Novoselov and co-workers in 2004 showed a novel approach to exfoliate a single flake of graphene by mechanical force. They found the layers were about 0.8nm in thickness as observed by atomic force microscopy (AFM)[21]. The main advantage of mechanical exfoliation was that the carbon layers were free of significant functional

groups and almost pristine. However the major setback with this method is the overall mass production is very low.

The scalability in production can be achieved best via chemical modification route starting from GO and reducing it which is known as reduced graphene oxide (r-GO). The resulting dispersions are typically very stable in water up to the concentration of 3-4 mg ml<sup>-1</sup>[64] primarily because of strong polarity of the oxide functional groups.

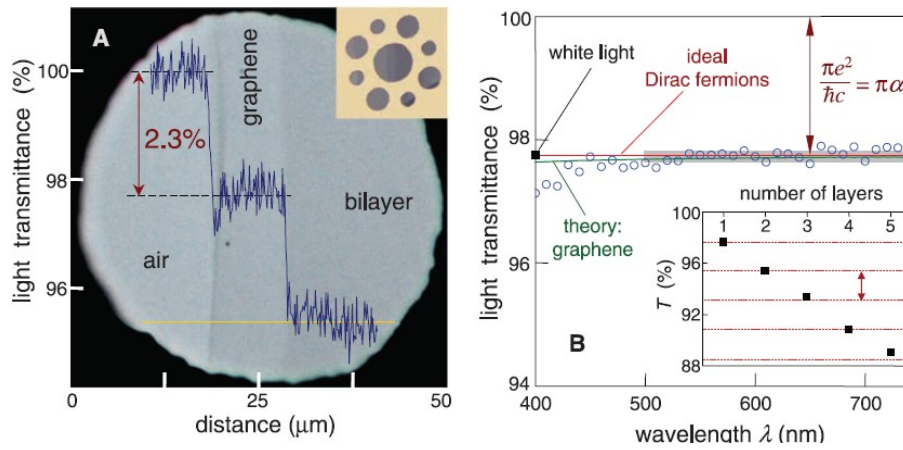


Figure 2-2: Visual transparency of graphene[67]. Reprinted with permission from AAAS.

One of the very unique properties of graphene is its tunable optical properties. Geim and co-workers observed a unique property of graphene which is a fundamental constant that does not depend on the material properties. They show the opacity of graphene is solely defined by the fine structure constant

$$\alpha = \frac{e^2}{\hbar c} \quad (2.1)$$

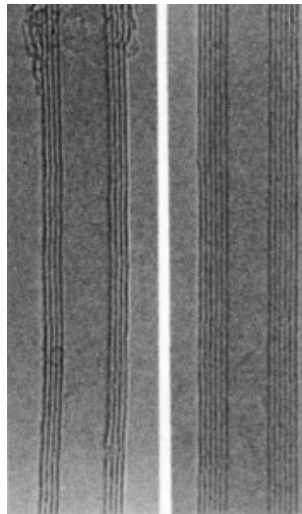
Where  $h$  is Planck's constant and  $c$  is speed of light

Despite being single layer atomically thick, graphene is found to absorb a significant fraction of white light.

In 2009 Geim and co-workers showed the extraordinary electronic properties of graphene at atomically small dimensions[22]. They observed that Dirac electrons behave in unusual way in tunneling, confinement and integer quantum Hall effect. They also observed that these electronic properties also changes with the change in the graphene stacking order and number of layers. It was also found that different types of disorders modify spectroscopic and transport properties of graphene.

## 2.2 Carbon Nanotubes

There are two main types of carbon nanotubes (CNTs), single walled nanotubes (SWNTs) and multi walled nanotubes (MWNTs) as shown in *Figure 2-3* where several SWNTs forms a concentrically nested like rings to form MWNTs.



*Figure 2-3*: Transmission electron microscope image of multi walled nanotubes comprised of an array of several single walled nanotubes. Image adopted from [68], Nature publishing group, copyright 1992.

SWNTs can be either metallic or semiconductor, depending on their chirality  $(n,m)$ , basically how graphitic single layered sheet is rolled to form a nanotube (NTs) cylinder. The NTs can either be armchair  $(n=m)$ , zigzag  $(n=0 \text{ or } m=0)$ , or chiral (*any other  $n$  or  $m$* ) variety. All armchair SWNTs are metals, those with  $n-m = 3k$ , ( $k =$  nonzero integer) are semiconductors.

The pristine metallic CNTs which are one dimensional electronic structure have superior electronic properties[69], [70]. It was found that the room temperature thermal conductivity for an MWNT was  $\sim 3000 \text{ W m}^{-1} \text{ K}^{-1}$ [71]. CNTs also have exhibited superior mechanical properties having high Young's modulus and high tensile strength. The Young's modulus of the CNT depending on its total area was found to be  $\sim 0.64 \text{ T Pa}$ [72]. Various techniques can be employed for the synthesizing nanotubes such as carbon-arc discharge, laser ablation of carbon or chemical vapor depositions (CVD).

### **2.3 High Surface Area Active Materials**

Graphitic carbons have proved in reaching high capacitance by charging the double layer using very high SSA blocking conductive electrode. Various types of carbons have been utilized and tested for EDLC applications such as activated carbons, nanotubes, carbon fabrics, etc[18] as shown in *Figure 2-4*.

Double layer capacitance of activated carbon reaches  $100\text{-}120 \text{ F g}^{-1}$  in organics electrolytes and their value may exceed  $150\text{-}300 \text{ F g}^{-1}$  in aqueous electrolyte. It has been shown previously that the untreated carbons have lower specific capacitance in the range of  $50\text{-}80 \text{ F g}^{-1}$  than activated carbon in organic electrolyte[46], [73].

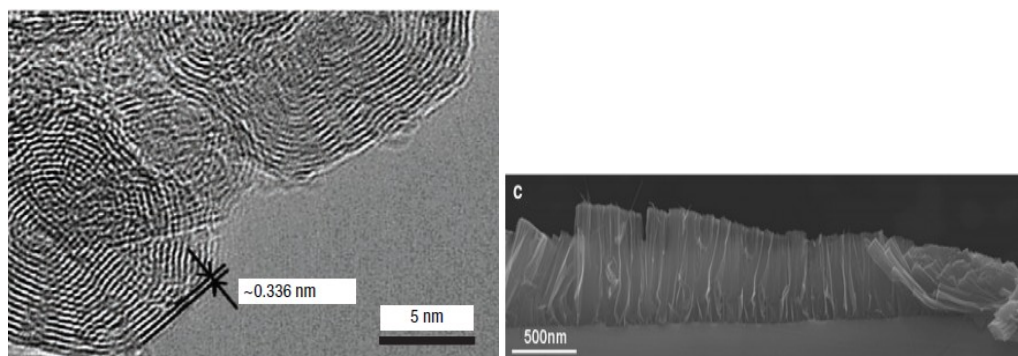
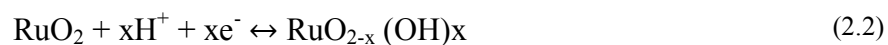


Figure 2-4: a) TEM image of onion-like carbon. Reprinted from [85] Copyright(2007), with permission from Elsevier, b) SEM of array of CNT on SiC. Reprinted from [127], copyright (2008), with permission from Elsevier.

Initial research was directed towards increasing pore volume by developing high SSA; however it was later observed that there is no linear relationship between the SSA and the capacitance[74], [75]. Studies suggest that pores small than 1nm were too small to be accessible by hydrated ions[74], [76]. Pore size distribution in the range of 2-5nm was seen to be a way to improve the capacitance. Gravimetric capacitance was seen in the range of 100-120 F g<sup>-1</sup> in organic and 150-200 F g<sup>-1</sup> in aqueous electrolytes[77], [78]. Fast reversible redox reactive materials are also used based on the pseudocapacitive behavior for energy storage applications. Metal oxides such as RuO<sub>2</sub>, Fe<sub>3</sub>O<sub>4</sub> or MnO<sub>2</sub>[79], [80] are some of the redox reactive materials as well as electronically conductive polymers[81]. Ruthenium oxide (RuO<sub>2</sub>) is widely because it is conductive within 1.2V. Fast reversible electron transfer together with an electro-adsorption of protons on the surface of RuO<sub>2</sub> particles.



Where  $0 \leq x \leq 2$ . A continuous change of  $x$  during proton insertion or de-insertion occurs over a window of 1.2V and leads to a capacitive behavior of about 600 F  $g^{-1}$ . The major drawback of Ru based capacitors is that they are very expensive.

## 2.4 Carbon based Nanocomposite

Owing to the large surface area, excellent electrical, mechanical, thermal and electrochemical properties carbon nanomaterial such as 1D carbon nanotubes [82]–[86] and 2D graphene [21], [22], [58] have been explored as an active materials for supercapacitor electrodes[87]–[90]. CNTs have been widely used as electrode materials with both liquid electrolytes and gel electrolytes[87], [91]. CNT can be brush/spray-coated on any non conductive surface such as paper cellulose and plastic film. It has been shown that CNT can be deposited on a bacterial nanocellulose substrate through vacuum filtrations. The assembled supercapacitors gave specific capacitance of 46.9 F  $g^{-1}$  at a scan rate of 0.1V  $s^{-1}$ [92]. In order to further improve the performance of CNT based supercapacitors, CNT composites with transition metal oxides and/or conductive polymers have been used to get the advantage of pseudocapacitance[93]–[95]. CNT coated with PANI also give reasonably very high specific capacitance of 350 F  $g^{-1}$  for the electrode materials and about 31.4 F  $g^{-1}$  for the entire device[96]. Along with the development and understanding of the CNTs use in supercapacitors, graphene is also been used as a potential materials for electrode[7], [97], [98]. The specific capacitances for most of the graphene based free standing materials are in the range of 80-118 F  $g^{-1}$ .

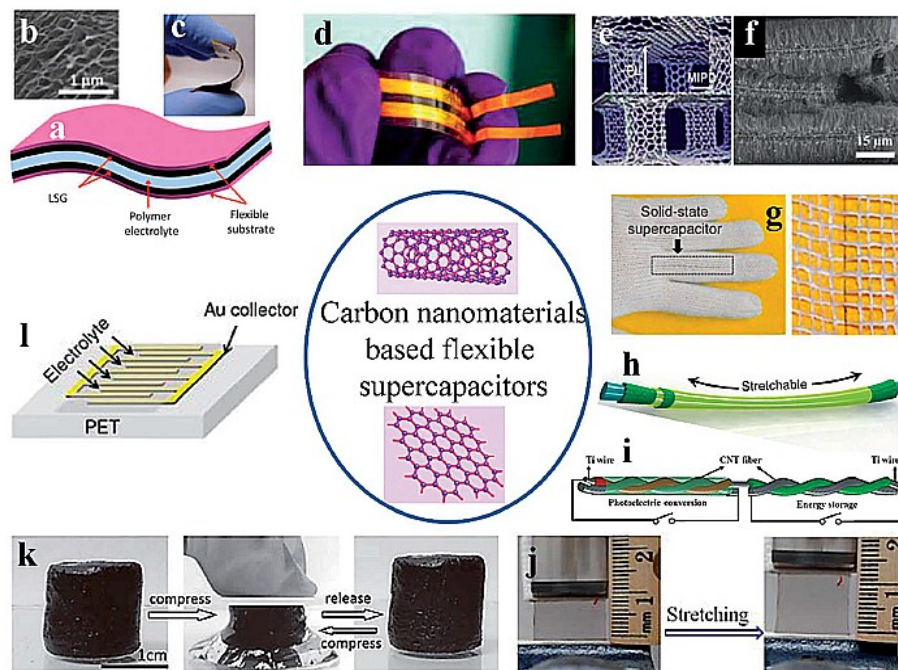


Figure 2-5 An overview of various carbon based nanocomposite supercapacitors of different structures and forms. Reproduced from [98] with permission of The Royal Society of Chemistry.

However, these values are much lower than the theoretical values of  $550 \text{ F g}^{-1}$ [2], mainly because of agglomeration of graphene flakes which greatly reduces the overall specific surface area of the composite.

One of the attractive options is to use the 1D CNTs to separate the 2D graphene flakes to preserve the high SSA of graphene and CNTs to make efficient electrolyte transport[87], [99]. The freestanding CNT/graphene hybrid film exhibited a nearly rectangular shape with specific capacitance of  $120 \text{ F g}^{-1}$  at  $1 \text{ V s}^{-1}$ [87]. Supercapacitors decorated with CNT and graphene on various textile materials like cotton and Kevlar also have been demonstrated[94], [100]–[102].



## 2.5 Cellulose as Substrate

Cellulose, a natural biopolymer, is by far the most abundant renewable polymer available today. Cellulose nanocrystals (CNs) have attracted the materials community because of its great chemical and physical properties, its renewability and sustainability leading to their low cost in various research applications. These self assembled biopolymers are available with variety of properties and forms from plants and organisms. Algae are thallophytes (plants lacking roots, stems and leaves) which grows in the water or lives close to it[103]. The fibrillar reinforcing component of algae cell walls is usually composed of cellulose. Cladophora species are green algae, found in freshwater and marine habitats, which can be a great source to extract highly crystalline cellulose[104].

Cellulose can be used from various other sources and it can be used as substrate for electrode fabrications having the advantage of making free standing binder-free electrodes for supercapacitor applications. Natural cellulose from paper has been used can coated with CNTs and depositing  $\text{MnO}_2$  composites achieving about  $300 \text{ F g}^{-1}$  at a low scan rate[105]. Graphene-cellulose nanocomposite flexible paper was reported by Weng and coworkers achieving gravimetric capacitance of  $120 \text{ F g}^{-1}$  and it retain the capacitance over 5000 cycles[106]. Cellulose as a substrate can be a great materials of a choice for making flexible free standing supercapacitors device.

## 2.6 Electrolytes

The supercapacitor cell voltage is directly dependant on the electrolyte stability at high potentials window. The cell voltage window of supercapacitors increases from 0.9V to 2.5V as we select from aqueous to organic electrolytes. As the energy density is directly proportional to the square of voltage applied, having a stable electrolyte at higher operating voltage is essential. Trend is to use the organic electrolyte solutions in acetonitrile (AC) or propylene carbonate (PC) to get the maximum voltage operating range. Ionic liquids are liquids at the room temperature which are solvent-free electrolytes. Hence the operating voltage window stability is thus driven by the electrochemical stability of ions[107]. Besides this people have shown the use of  $\text{H}_2\text{SO}_4$ [88], aqueous solutions of  $\text{KOH}$ [108],  $\text{Na}_2\text{SO}_4$ [99],  $\text{NaCl}$ [109].

## **CHAPTER 3. GOALS OF RESEARCH**

The goal of my thesis work is to fabricate and analyze two kinds of nanocomposite electrodes for supercapacitor application.

- 1) Fabrication of template electrode: Synthesis of algae cellulose-polypyrrole-graphene nanocomposite as an electrode for supercapacitor application.
- 2) Fabrication of hybrid template-less electrode: Synthesis of substrate-less free standing polypyrrole-graphene- CNT nanocomposite film as an electrode for supercapacitor application.
- 3) Detailed electrochemical analysis of both templated and template-less electrodes in presence of various electrolytes.
- 4) Device fabrication and analysis and performance test using a light emitting diode and comparison with existing commercial technologies such as alkaline battery and conventional supercapacitor.
- 5) Fabrication of unique nanofibrous separator membrane using electrospinning.

To accomplish the goals various experimental techniques and equipments to characterize the supercapacitor electrode will be used such as Scanning Electron Microscope (SEM), Transmission Electron Microscope (TEM), UV-Raman spectroscopy and Cyclic Voltammetry (CV).

# **CHAPTER 4. SYNTHESIS AND ELECTROCHEMICAL ANALYSIS OF ALGAE CELLULOSE-POLYPYRROLE- GRAPHENE NANOCOMPOSITE FOR SUPERCAPACITOR ELECTRODE**

## **4.1 Electrode Fabrication**

A detailed description of the electrode fabrication is as follows:

### **4.1.1 Cellulose Extraction**

We used *c. aegagropila* algae balls to extract the cellulose from it. 50g of algae was bleached using 18g of NaClO<sub>2</sub> (sodium chlorite) in acetic buffer to wash away the impurities. The mixture was diluted to 50ml and stored in a water bath for 2hr. The product was then neutralized with de-ionized (DI) water. 300ml of 0.10M NaOH (sodium hydroxide) was added to the beaker and stored overnight.

The pulp was then neutralized with DI water, dried, ground and hydrolyzed by heating with H<sub>2</sub>SO<sub>4</sub> (sulfuric acid) in order to depolymerize the plant fibers. The pulp was then allowed to stand overnight and then washed to neutrality with de-ionized water to end the hydrolysis process (*Figure 4-1*).



Figure 4-1: A) Optical image of algae ball prior to cellulose extraction, B) Algae cellulose extracted in pulp form after the hydrolysis, C) Filtered cellulose pulp

### 4.1.2 Graphene synthesis and processing

Graphene was synthesized from graphene oxide in its reduced form called reduced graphene oxide (r-GO). Graphene solution was prepared by measuring known amount of graphene oxide powder mixed in water to make solution of 0.01 wt%. The solution is sonicated for at least 2 hr with little heat applied (*Figure 4-2*).

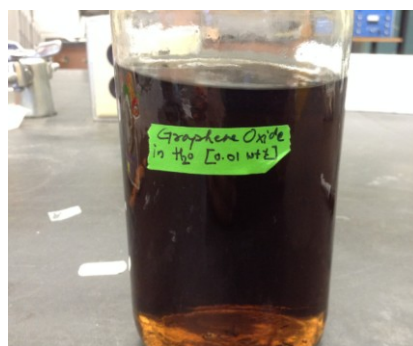


Figure 4-2: Graphene oxide solution after sonication for 2hr.

Graphene can be reduced from as prepared graphene oxide as follows:

- 1) GO (100mg) was loaded in 100ml water followed by the sonication in water bath until the solution becomes clear with no visible particulate matter.
- 2) Hydrazine hydrate 1ml was then added and the solution was heated at 100°C for 24 h.

The resultant product will be black solid which is reduced graphene oxide filtered. In order to utilize the ballistic conductivity of the graphene as a component of the electrode, it is very important to have the total SSA as high as possible. But one of the major challenges with using graphene is that it tends to agglomerate and hence yields very low SSA.

To have a uniform dispersion, graphene was dispersed in TE buffer as follows:

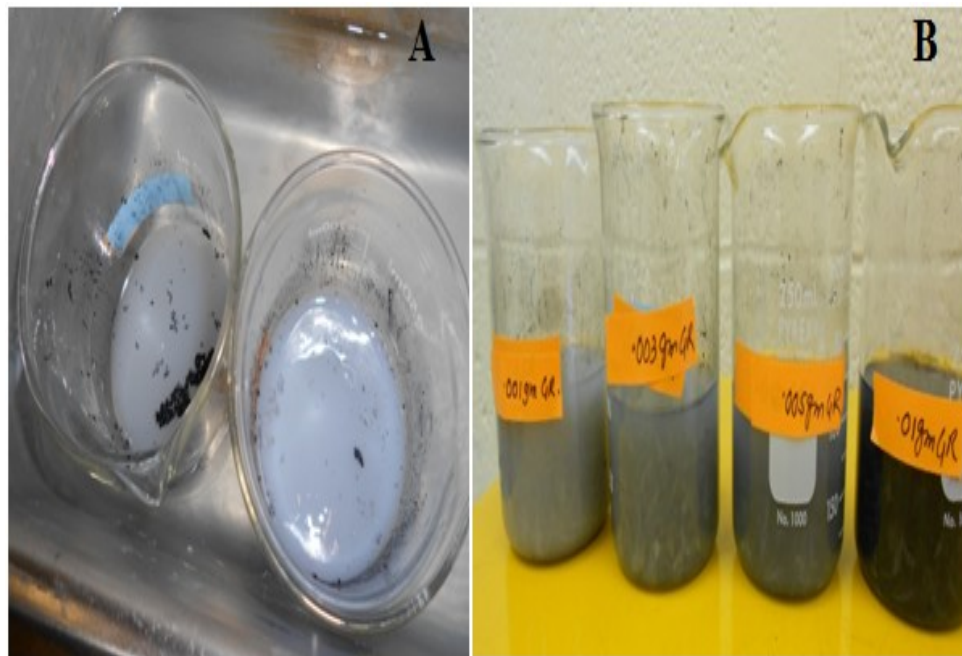
A 100 ml of 7X TE (Tris-EDTA) buffer solution was prepared by mixing 6.55 ml Tris (TEKnova, 1M, pH 7.5) and 1.3ml EDTA (Promega Inc. 0.5M, pH 8.0) solutions together in 1X TE (0.01M Tris and 0.001 M EDTA, pH 7.4) buffer. 1 mg graphene powder was added in 7 X 10ml TE buffer solutions and it was sonicated for at least 2 hrs with heating until we see the graphene powder is well dispersed in the solution without any agglomeration.

### **4.1.3 Polymerization of Pyrrole**

To evaluate the performance of different types of electrodes and to see the effect graphene, various nanocomposites were fabricated using varying concentration of graphene. Graphene was added prior to doing the polymerization step of Py. After the

extraction of cellulose from algae in form of pulp addition of Py was performed as follows.

### *Addition of graphene*

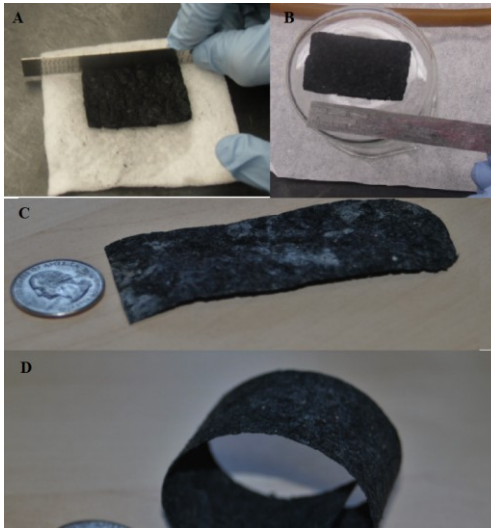


*Figure 4-3: A) Solution preparation of Py and Tween80 with varying concentration of graphene, B) Cellulose pulp addition to Py solution containing Tween80 and graphene.*

Graphene nanoplateletes with varying concentration (1mg and 3mg) were dispersed in 10ml Py solution in presence of 1 $\mu$ l of polysorbate (Tween-80) surfactant for better dispersibility and adsorption on the cellulose. The solution was sonicated for 1 hr. The cellulose pulp was mixed with Py solution and then collected on filter paper as shown in *Figure 4-3*. 8g of FeCl<sub>3</sub> was dissolved in 100 ml of distilled water and run through the pulp to induce the polymerization for 10 min. A sponge like cake was formed at the end of polymerization process.

#### 4.1.4 Nanocomposite Paper Fabrication

After the formation of sponge like cake containing cellulose pulp coated with PPy and varying graphene concentrations, the mixture was filtered on polypropylene filter. The final product was dried and it was given a rectangular shape with approximate thickness of 100 $\mu$ m as shown in *Figure 4-4*



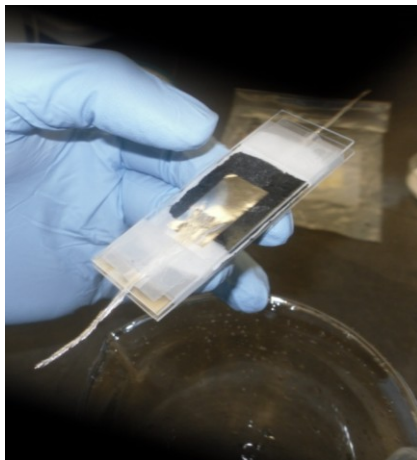
*Figure 4-4:* Optical images of various stages of conductive paper fabrication. Image (A, B) Cellulose coated with PPy and graphene being given a rectangular shape by applying pressure in order to get desired thickness. Image (C, D) Final conductive paper electrode without and with graphene respectively.

#### 4.1.5 Supercapacitor Device Assembly

The supercapacitor unit cell was assembled as shown in *Figure 4-5*. The assembly was made symmetrically having conducting nanocomposite electrodes on each side. Care is taken to keep these two electrodes separate using a separator such as a whatman filters paper. 1M NaCl is used as an electrolyte and the separator is soaked with it. Platinum (Pt)



is used as a current collector which is attached to the electrode on the top surface and it is used as a connector to connect the device.



*Figure 4-5: Picture of supercapacitor device made from conducting nanocomposite electrodes.[110]*

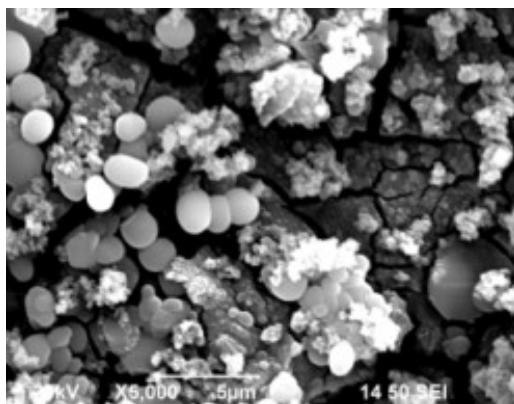
## **4.2 Characterization Techniques**

### **4.2.1 Scanning Electron Microscopy (SEM)**

Scanning electron microscopy (SEM) was a very useful tool to observe and image the morphology of various nanomaterials of the electrode such as graphene, polypyrrole (PPy) and algae derived cellulose.

#### **4.2.1.1 Graphene Oxide SEM**

SEM was performed on the graphene oxide to observe the structural morphology. SEM is a very useful tool to visualize the surface morphology of the sample under investigation. A dispersed graphene oxide solution with the concentration of 0.16 mg/ml was drop casted on SEM stub and dried for 3hr.



*Figure 4-6:* SEM micrograph of graphene oxide with the concentration of 0.16 mg/ml at magnification of x5000, revealing a typical platelet like structure. [111]

Figure 4-6 shows a typical image of graphene oxide flakes. The flakes are held together by surface tension in a small drop of graphene oxide solution and while drying generally the flakes agglomerate together. SEM micrograph is taken at x5000 magnification with the scale bar of 5µm.

#### **4.2.1.2 Graphene Nanoplateletes SEM**

SEM was used to observe the structural morphology of graphene when dispersed in TE buffer. Graphene was dispersed in TE buffer with the concentration of 1mg/ml. It was followed by sonication for about 45 min which developed a homogenously well dispersed black color solutions. Dispersed graphene solution was drop casted on SEM stub to capture the images. *Figure 4-7* shows a typical image of graphene flakes. Small individual graphene flakes are held together by van der Waals forces and surface tension in a small drop of graphene solution. SEM micrograph is taken at various magnifications.

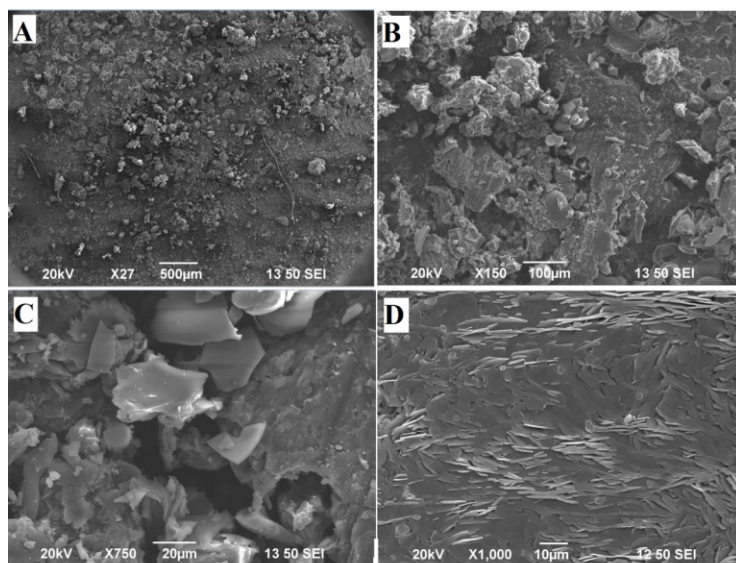


Figure 4-7: SEM micrograph of graphene nanoplatelets dispersed in 7X Tris-EDTA buffer [111]

#### 4.2.1.3 Cellulose Paper Nanocomposite SEM

SEM image of the nanocomposite paper electrode was taken to see the surface morphology and the effect of polymerization on the cellulose fibers. *Figure 4-8* shows an interesting beaded morphology of tween 80 surfactant self-assembled in a “necklace” like structure. Beaded morphology starts to break upon increasing the concentration of graphene in the overall matrix. Polysorbate-80 was used as a surfactant to enhance the adsorption of pyrrole to the cellulose fibers. Since only a small quantity is required for effective adsorption of pyrrole to the surface of cellulose, the remaining amount might have been utilized by nonpolar graphene flakes, which attract to the hydrophobic tails of the polysorbate-80 molecule.

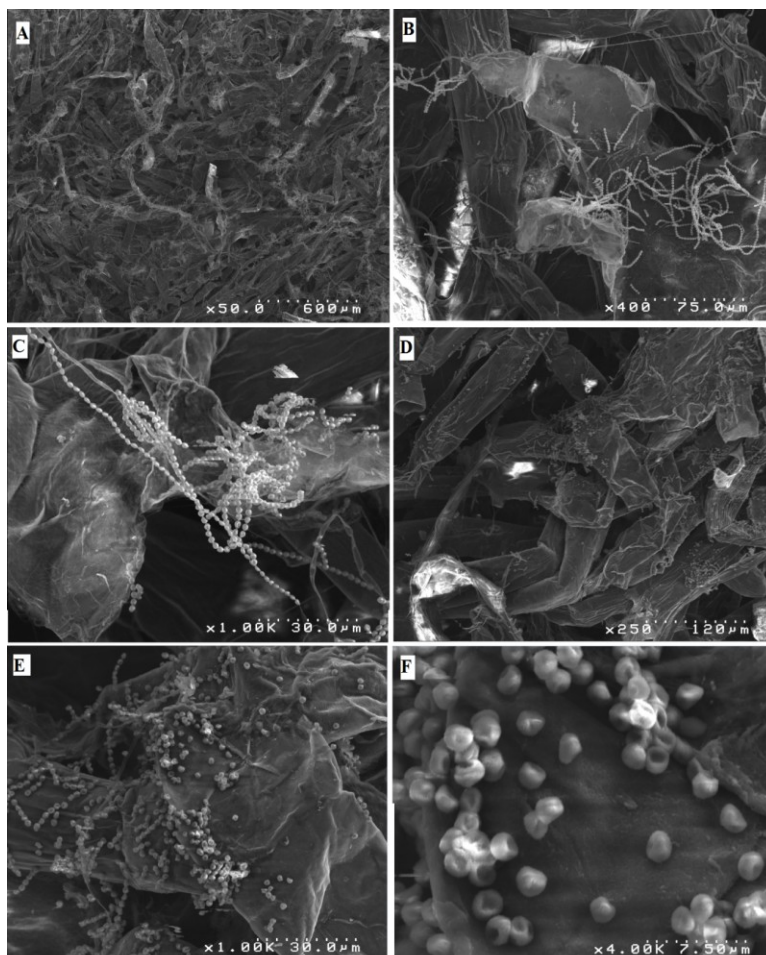


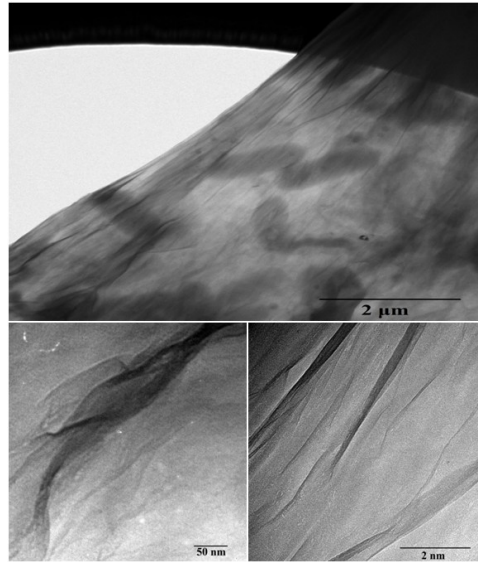
Figure 4-8: SEM micrograph of nanocomposite with cellulose fibers coated with no graphene (A-C) and with 0.01 wt% graphene (D-F)[110]

#### 4.2.2 Transmission Electron microscopy (TEM)

TEM is very powerful instrument and imaging technique which allows the samples to be imaged at close to 1nm range. TEM was used to observe the graphene oxide, graphene and the nanocomposite samples dispersed in their respective solvents. A drop was casted on TEM grid and dried overnight ready to be used in TEM.

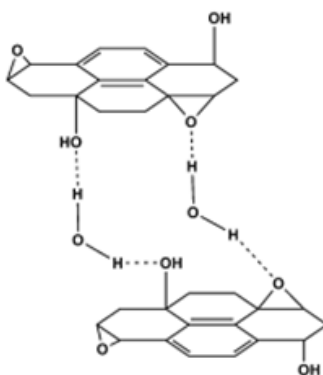
#### 4.2.2.1 Graphene oxide TEM

Graphene oxide powder was dispersed in water at 10mg/ml concentration followed by sonication for about 3 hrs. *Figure 4-9* shows the TEM image of graphene oxide captured at various magnifications.



*Figure 4-9:* TEM micrograph of graphene oxide dispersed in water by sonication.

It is clearly seen through the TEM image the single flake of graphene oxide and its wrinkles on the surface. Graphene oxide is very easily dispersible in water since it has oxygen and other types of functionalities on its surface and edges. Nitric acid is a common oxidizing agent and is known to react strongly with aromatic carbon surfaces, and the reaction results in formation of various oxides containing species including carboxyl, lactones and ketones. The starting material for such reaction is taken as graphite flakes, which consists of numerous defects in the  $\pi$ -structure, which may serve as a seed point for the oxidation process[112].



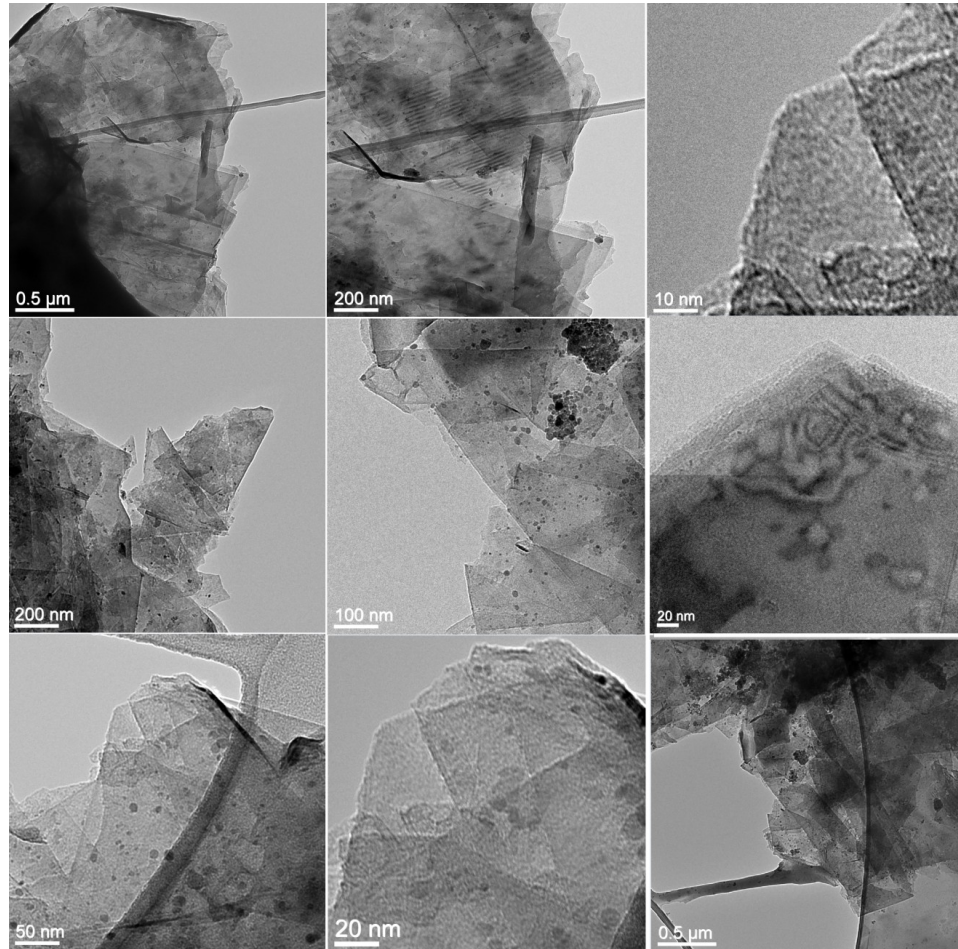
*Figure 4-10:* Proposed hydrogen bonding network formed between oxygen functionality on GO and water. Reproduced from [112] with permission of The Royal Society of Chemistry (RSC).

In case of graphene oxide rather than retaining a stacked structure, the material is exfoliated into monolayer. The surface functionalities greatly weaken the platelet-platelet interactions, owing to its hydrophilicity. There are different methods to exfoliate the graphene oxide layers either by mechanical stirring or sonicating. Sonicating is faster method but it will cause substantial damage to the graphene oxide platelets[113]. The dimensions of these particles are diminished to several hundred nanometer per side [114]. The oxidation process itself also causes breaking of the graphitic structure into smaller fragments.

#### 4.2.2.2 Graphene TEM

In order to observe the structure of graphene flakes and its size TEM was performed. A drop of graphene dispersed in 7xTE buffer solution was casted onto the TEM grid and dried overnight. This TEM grid was used to image the graphene flakes. As seen above in *Figure 4-11*, we can see the individual graphene flakes that are exfoliated during long time of sonication. It is evident from the previous literature[67] that as the

number of layers of the overall graphene flake reduces the whole structure starts to become more and more transparent.

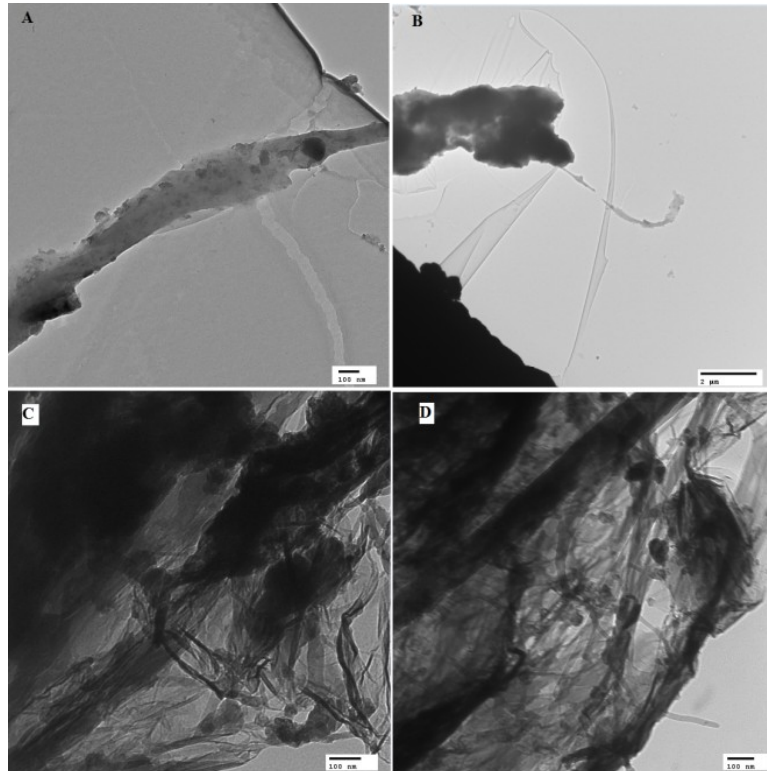


*Figure 4-11: TEM micrograph of graphene dispersion in 7X TE buffer.*

As seen in *Figure 4-11*, it is clearly observed that certain area have stacked layers of graphene and they are less transparent compared to the area where there are less layers of graphene. We can also derive a conclusion that giving enough sonication time for the stacked graphene solution, graphene layers can be exfoliated to few numbers of layers, hence increasing the overall SSA of the sample.

### 4.2.2.3 Paper Nanocomposite TEM

To observe that effect of the PPy polymerization on the overall nanocomposite matrix, TEM was performed on two samples, cellulose-PPy graphene (0g) and cellulose-PPy-graphene (5mg).



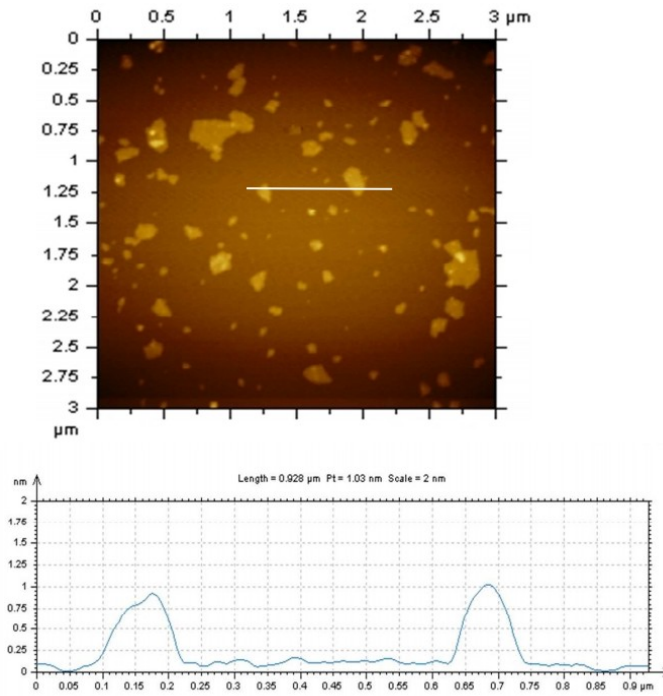
*Figure 4-12: TEM micrograph of cellulose-PPy-graphene nanocomposite, (A,B) cellulose-PPy, (C,D) cellulose-PPy-graphene (0.005g) [110]*

It can be clearly observed that the coating and extent of PPy polymerization on each cellulosic fiber has been well done. It can also be seen that the average diameter of these cellulose fibers is roughly in the range of 500nm. However there are bigger fibers as well in micron range.



### 4.2.3 Atomic Force Microscopy (AFM)

AFM was utilized to study the morphology of graphene oxide and to verify its single layer morphology. Graphene oxide powder was dispersed with the concentration of  $15\mu\text{g/ml}$  in water and sonicated for 2 hrs.  $5\mu\text{L}$  of aqueous graphene oxide dispersion was spread onto a freshly cleaved mica surface and left to dry in air.



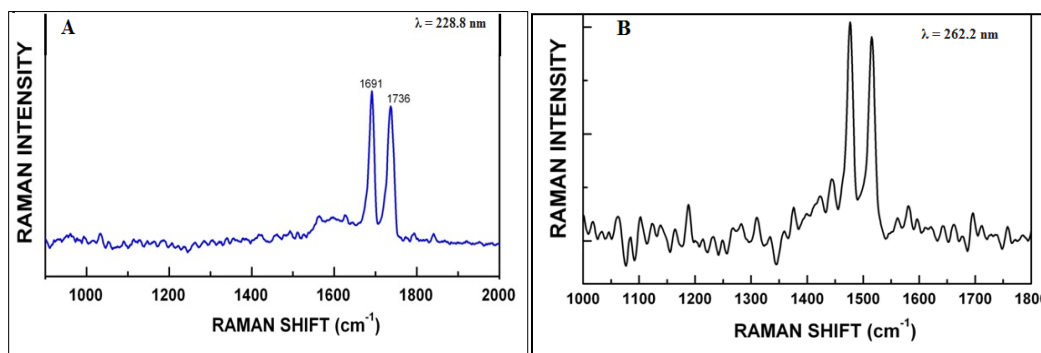
*Figure 4-13:* Tapping mode AFM image of graphene oxide deposited on a freshly cleaved mica surface with height of  $\sim 0.9\text{nm}$  [115]

### 4.2.4 UV-Resonance Raman Spectroscopy (UVRR)

Graphitic materials have been typically characterized by a highly dispersive band in the  $1200\text{-}1400\text{ cm}^{-1}$  region, called the disorder-induced D band and the graphitic mode (G) at higher frequencies ( $\sim 1590\text{ cm}^{-1}$ ) related to the primary in-plane vibrational mode

within the graphene sheet. Additionally functionalization of graphene has also been found to profoundly affect the frequency of the G band along with the number of layers[116].

The UV resonance Raman spectra (*Figure 4-14, A*) of graphene dispersions were done at  $\lambda_{\text{exc}} \sim 228$  nm. Raman spectra collected for the functionalized graphene nanoplateletes dispersion shows two very distinct bands are noted at  $1691\text{ cm}^{-1}$  and  $1736\text{ cm}^{-1}$ .



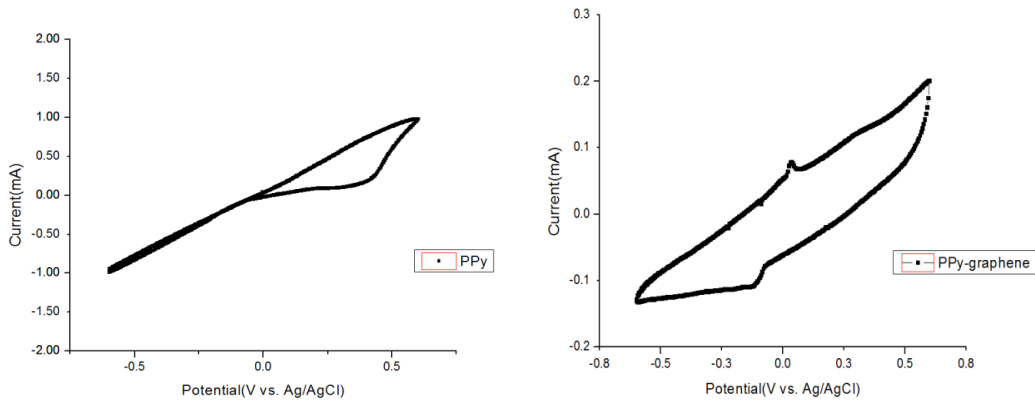
*Figure 4-14:* UV-Raman spectra of graphene dispersed in 7x TE buffer [111]

*Figure 4-14 B*, represents the UV resonance Raman spectra of the graphene dispersions at  $\lambda_{\text{exc}} \sim 262$  nm. It is interesting to note that similar to the spectra collected at 228 nm, two very sharp bands are noted in the graphene nanoplateletes dispersion however at lower frequencies ( $\sim 1477\text{ cm}^{-1}$  and  $1516\text{ cm}^{-1}$ ).

### 4.3 Electrochemical Analysis of the electrode

The electrochemical response of the PPy-cellulose and PPy-graphene- cellulose electrodes was determined from cyclic voltammetry measurement. The working electrodes (WE), PPy-cellulose or PPy-graphene-cellulose with thickness of  $100\mu\text{m}$  and

0.64 cm<sup>2</sup> area were used to perform electrochemical studies. *Figure 4-15* (A, B) shows the voltammogram plots at 50 m V s<sup>-1</sup> scan rate of both nanocomposite electrodes. The PPy-cellulose electrode weighs about 7.2 mg and PPy-graphene-cellulose weight was 6mg.



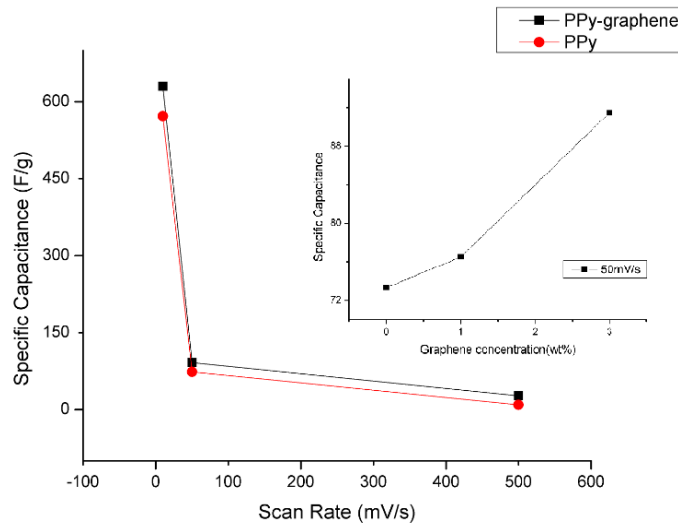
*Figure 4-15:* Cyclic voltammetry curves obtained using A) PPy-cellulose, B) PPy-graphene-cellulose nanocomposite at scan rate of 50 m V s<sup>-1</sup> in aqueous 1M NaCl electrolyte. [110]

The specific capacitance of the electrodes have been determined using following equation[108].

$$C = \frac{1}{2mVs} \int_{V_-}^{V_+} I(V)dV \quad (4.1)$$

Where  $C$  is the specific capacitance (F g<sup>-1</sup>),  $m$  is the mass of electrode (g), [ $V = V_+ - V_-$ ] the potential difference and  $s$  is the scan rate (m V s<sup>-1</sup>). The specific capacitance of the PPy-cellulose electrode was 73.32 F g<sup>-1</sup> at the scan rate of 50 m V s<sup>-1</sup> and PPy-graphene-cellulose electrode has 91.5 F g<sup>-1</sup>.

The variation in the specific capacitance of PPy-cellulose and PPy-graphene-cellulose nanocomposite as a function of scan rate is shown in *Figure 4-16*. At the scan rate of  $10\text{mVs}^{-1}$  the specific capacitance of PPy-cellulose nanocomposite is  $572\text{ F g}^{-1}$  and that of PPy-graphene-cellulose is  $630\text{ F g}^{-1}$ . At  $50\text{ m V s}^{-1}$  the specific capacitance of PPy-cellulose nanocomposite is  $73.32\text{ F g}^{-1}$  whereas PPy-graphene-cellulose gives  $91.5\text{ F g}^{-1}$ . The specific capacitance of the nanocomposite goes higher at low scan rates because the  $\alpha\text{-C}$  atoms of the PPy ring have been almost oxidized to form C-C bonds in the process of polymerization. So some  $\alpha\text{-C}$  at the end of polymer chain and  $\beta\text{-C}$  atoms of the PPy chains could be oxidized / deoxidized. When the scan rate is low, these atoms are not only oxidized/deoxidized, but also the doping ions have enough time to inject/eject from the PPy particles freely[117]. *Figure 4-16*(inset) shows the specific capacitance of the nanocomposite with varying graphene concentration. At a scan rate of



*Figure 4-16*: Variation of specific capacitance of PPy-cellulose and PPy-graphene-cellulose nanocomposite as a function of scan rate. (Inset: Specific capacitance change as function of graphene concentration at scan rate of  $50\text{ mVs}^{-1}$ )[110]

50 m V s<sup>-1</sup> nanocomposite without graphene (0 g) has specific capacitance of 73.32 F g<sup>-1</sup>, nanocomposite with 1 mg graphene has 76.49 F g<sup>-1</sup> and with 3mg of graphene the specific capacitance was 91.5 F g<sup>-1</sup>. An increasing specific capacitance trend is observed with the increase in graphene concentration in the nanocomposite.

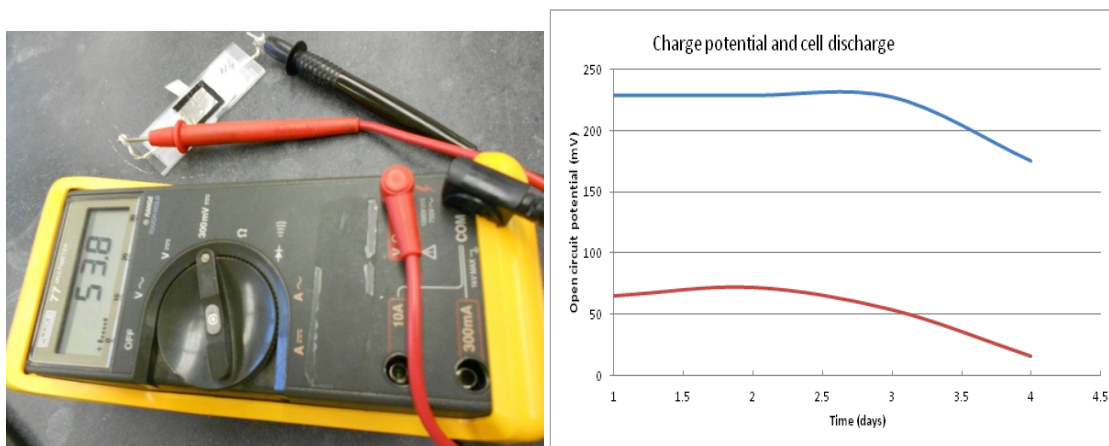


Figure 4-17: Supercapacitor reading using multimeter recorded over 4 days. [110]

Multimeter was used to measure electrical potential of the nanocomposite devices. The self-discharge rate of the devices was investigated by measuring the open circuit voltages for several days. *Figure 4-17* illustrates the full potential of the PPy-graphene- cellulose device was approximately 3.5 times that of the PPy- cellulose device. It is apparent that device containing PPy- cellulose electrodes started to discharge after about two days, whereas the device containing PPy-graphene-cellulose electrode began discharging after about three days.

# **CHAPTER 5. A NOVEL TEMPLATE-LESS HYBRID NANOCOMPOSITE ELECTRODE FOR SUPERCAPACITOR**

A detailed description of fabrication of a unique template-less free standing electrode film made from polypyrrole- CNT and graphene nanocomposite has been presented below.

## **5.1 Nanocomposite electrode fabrication**

### **5.2 Materials and methods**

#### **5.2.1 Pyrrole solution:**

To prepare the sample, 200ml of deionized water was measured and added to it 6.982ml of Py with 2.84 g of sodium sulfate ( $\text{Na}_2\text{SO}_4$ ). Stir the solution for 30min with no heat, until the solution is clear and homogenous.

#### **5.2.2 Pyrrole-graphene-CNT (PCG) solution:**

To compare the effect of graphene and CNT in the overall nanocomposite matrix of PPy and unique solution of PPy containing graphene and CNT was prepared. To further observe the effect of the graphene and CNT concentration on the overall energy

storage different solutions were prepared by measuring individual samples of graphene and CNT and mixing it with PPy solution.

### **5.2.3 Graphene and carbon nanotube:**

Graphene was synthesized from graphene oxide in its reduced form called reduced graphene oxide (r-GO). Graphene solution was prepared by measuring known amount of graphene oxide powder mixed in water to make solution of 0.01 wt%. The solution is sonicated for at least 2 hr with little heat applied.

Graphene can be reduced from as prepared graphene oxide as follows:

- 1) GO (100mg) was loaded in 100ml water followed by the sonication in water bath until the solution becomes clear with no visible particulate matter.
- 2) Hydrazine hydrate 1ml was then added and the solution was heated at 100°C for 24 h.

The resultant product will be black solid which is reduced graphene oxide filtered.

In order to utilize the ballistic conductivity of the graphene as a component of the electrode, it is very important to have the total SSA as high as possible. But one of the major challenges with using graphene is that it tends to agglomerate and hence yields very low SSA.

Carbon nanotubes were purchased from Cheaptubes Inc. They were used as it is without any further treatment.

## 5.2.4 Polymerization of Pyrrole and nanocomposite solutions

A novel hybrid electrode from PPy - graphene - CNT has been fabricated using electropolymerization method. The final product is a free standing film that can be used as an electrode for the supercapacitor application. Potentiostat deposition technique was used to fabricate PPy and PPy-graphene-CNT nanocomposite film on the graphite electrode. Pyrrole is known to polymerize under potential of 800 m V.

Table 5-1: Cyclic voltammetry parameters for depositing pyrrole and pyrrole-CNT-graphene nanocomposite free standing films

CV parameters	Pyrrole (Py)	Pyrrole-graphene-CNT (PCG)
$V_{\max}$ (mV)	900	900
$V_{\min}$ (mV)	800	800
Scan rate (mVs <sup>-1</sup> )	20	10
Cycles	100	100

Using three electrode setup where the working electrode (WE) is either graphite/gold/Pt, reference electrode (RE) is Ag/AgCl and counter electrode (CE) is platinum (Pt) in pyrrole solution. Potential is swept from 900 m V to 800 m V at a scan rate of 10 m V s<sup>-1</sup>



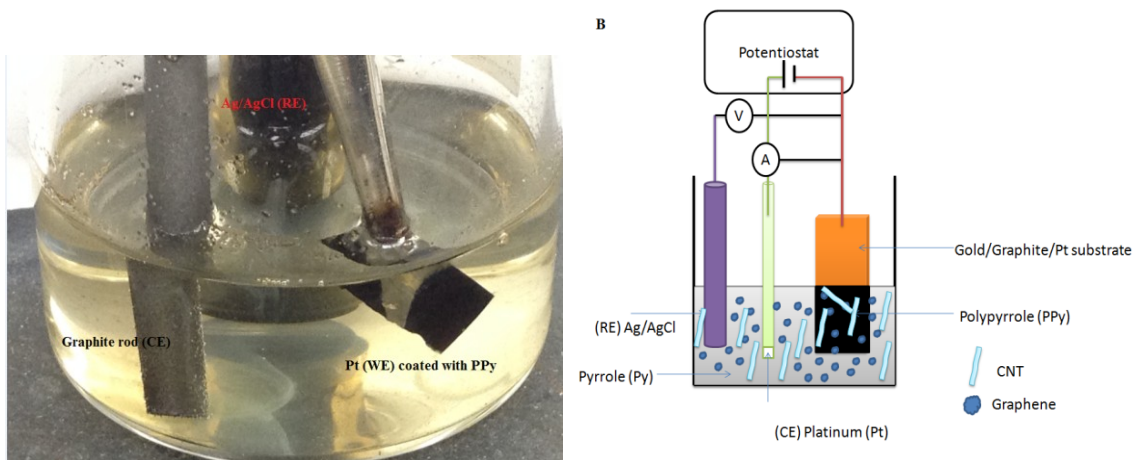


Figure 5-1: Polymerization of pyrrole using three electrode setup CV with Pt (WE), graphite rod (CE) and Ag/ AgCl (RE)

### 5.2.5 Fabrication of Freestanding Nanocomposite Film

After setting up the cyclic voltammetry setup as described in the above section and running the potentiostat for 100 cycles the pyrrole monomer starts to get polymerize forming a long chain of conductive polypyrrole.

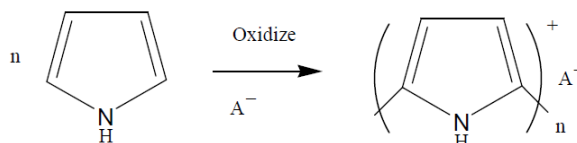


Figure 5-2: Polymerization of pyrrole (Py) to conductive polymeric chain of polypyrrole (PPy)

During polymerization of pyrrole, electroneutrality of the polymer matrix is maintained by incorporation of anions (called dopants) from the reaction solution, corresponding to one anion for every 3-4 monomer units, making upto 30-40% of the

final weight of the polymer depending on the type of the dopant anion. A simple model of pyrrole polymerization is shown in Figure 5-2.

Here  $A^-$  is the counterion incorporated into the polymer during polymerization in order to achieve electroneutrality[118]. A counter ion stabilizes the charge on the polymer but is not very mobile within the dry material. Thus these polymers are truly electronic and ionic conductors[119]. This long chain of polypyrrole gets deposited on the graphite which is negatively charged. Now this film can be easily peeled off after the 100 cycles has finished and these freestanding films can be used as an electrode for supercapacitor applications.



*Figure 5-3:* Optical images of PPy film formation on graphite substrate. A free standing film can be peeled off to be used as an electrode. A) Control PPy film, B & C) PPy-graphene-CNT film.

### 5.2.6 Electrolyte comparison

The supercapacitor cell voltage is directly dependent on the electrolyte stability at high potentials window. As the energy density is directly proportional to the square of voltage applied, having a stable electrolyte at higher operating voltage is essential. The performance of electrodes was studied using different electrolytes such as ascorbic acid (AA), sodium sulfate (SS) and sulfuric acid (SA). AA electrolyte was prepared using 10mM Ascorbic Acid+50mM Phosphate Buffer Saline (PBS). The AA which is also known as Vitamin C is an example of weak electrolytes but it occurs naturally and is very biosafe. On the other hand the SS is an example of strong electrolyte which is aqueous in nature. It can be prepared by adding weighted amount of sodium sulfate salts in the deionized water. As it is neutral salt, its pH is very near to 7. And SA is also a strong electrolyte with the pH of 1M of  $H_2SO_4$  close to 0.

## 5.3 Scanning electron microscopy

After the nanocomposite electrode films were fabricated, a detailed SEM was performed to observe the morphological structure of the complete electrode.

### 5.3.1 Polypyrrole

As seen in the *Figure 5-4*, a typical “cauliflower” structure of the PPy which has nucleated to form various grains. The average diameter of each individual grain size is approximately  $6\mu m$ . At the surface of the PPy film such grains binds together and that is where they form the pores. The average size of these pores in the PPy structure is  $\sim 300nm$  in diameter.

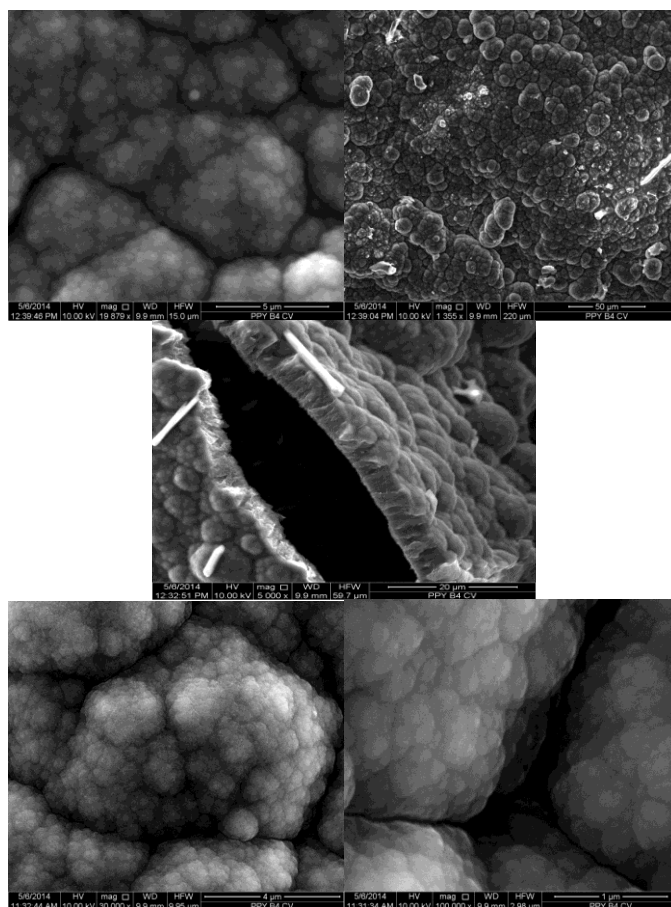
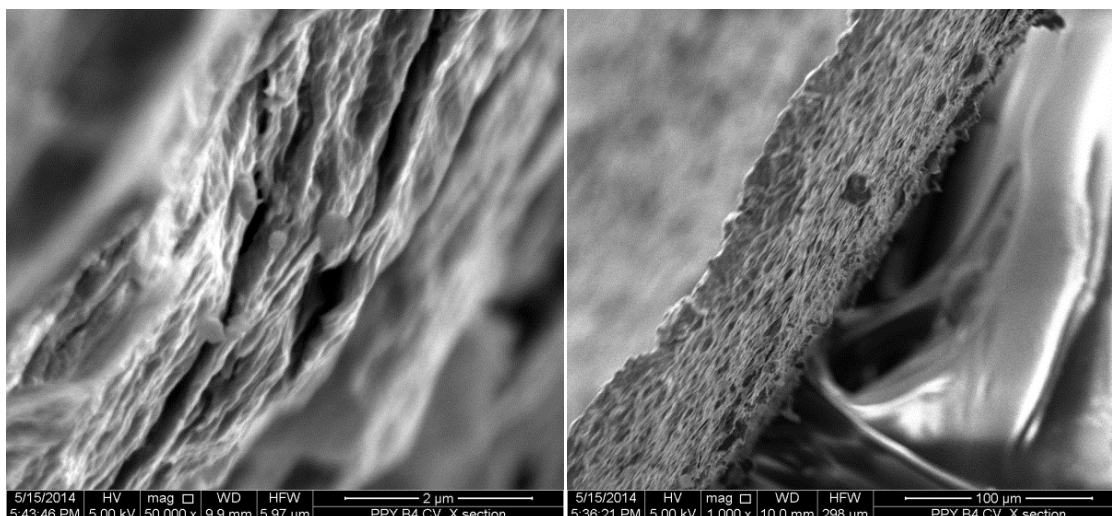


Figure 5-4: SEM micrographs of control PPy electrodes at various magnifications

### 5.3.2 Cross section of Polypyrrole films

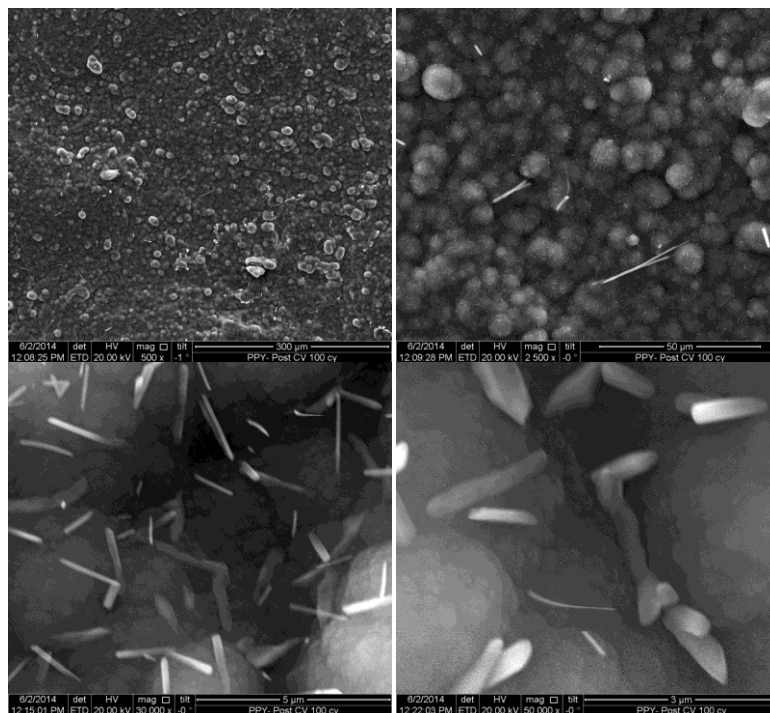
The cross sectional micrograph images of PPy reveal the thickness of the nanocomposite films after 100 cycles of deposition. The average thickness of the PPy film is  $\sim 70 \mu\text{m}$ . Very interesting flakes of several individual layers of PPy can be seen in the cross sectional image using SEM. The approximate distance between two layers is 120 nm and the thickness of the each individual layers is  $\sim 130 - 250 \text{ nm}$ , suggesting extremely small pores formation in the PPy structure. This small pores formation basically leads to the high specific surface area of the electrode material which allows it to store higher charges on its surface.



*Figure 5-5:* Cross- sectional SEM micrographs of PPy

### **5.3.3 Scanning electron microscopy of Polypyrrole after 100 cycles of cyclic voltammetry in sodium sulfate electrolyte**

As seen in the *Figure 5-6*, several needle like structures are observed on the surface of the PPy film after performing the cyclic voltammetry for approximately 100 cycles. This suggests the effect of electrochemical activity occurring on the surface of polypyrrole and perhaps the degradation of the PPy film after 100 cycles. It is seen that several needle like structures emerges on the PPy surface and they also can be seen overall at the pores as well. These needles like structures could be the results of SS salt which might have agglomerated on the surface after about 100 cycles. The approximate length of this needle like structures is about 1000 nm with the width of 300nm.



*Figure 5-6:* Needle like structures seen in the SEM micrograph of the controlled PPy film after performing cyclic voltammetry in 1M Na<sub>2</sub>SO<sub>4</sub> (SS) electrolyte, suggesting the degradation of the polymer film over the time.

### 5.3.4 Scanning electron microscopy of Polypyrrole-graphene-CNT nanocomposite electrode after 100 cycles of cyclic voltammetry in sodium sulfate electrolyte

Cyclic voltammetry was also performed on the PCG0.01 sample for 100 cycles to see the effect of the polymer degradation in Na<sub>2</sub>SO<sub>4</sub> electrolyte. As it is seen in the *Figure 5-7*, after the cyclic voltammetry done Na<sub>2</sub>SO<sub>4</sub> electrolyte there is a clear visible nanocubes instead of needles as observed in the PPy nanocomposite. The average size of the nanocubes is ~80nm.

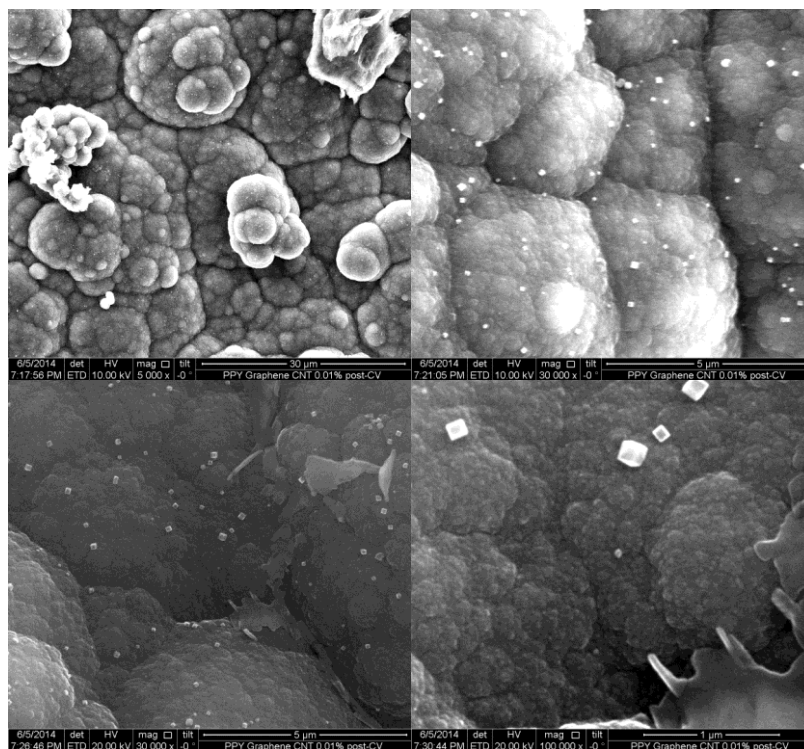


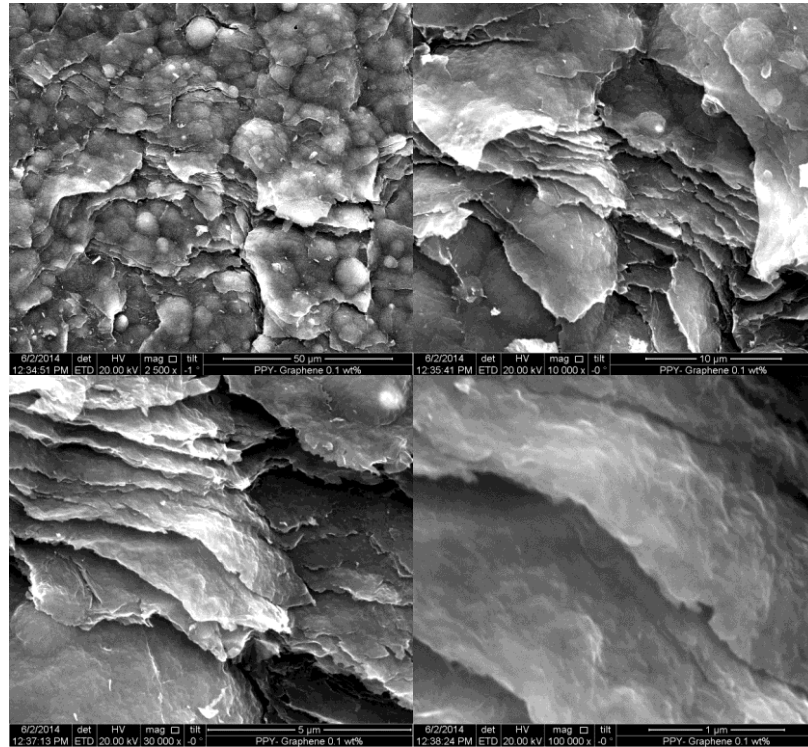
Figure 5-7: SEM images of post CV done for 100 cycles to observe the degradation in the samples of PCG0.01

### 5.3.5 Polypyrrole-graphene nanocomposite electrode (PG)

Further to investigate the effect of addition of graphene in the matrix of PPy, a measured quantity of graphene was added to the already prepared Py solution making it to 0.1 wt% concentration of the overall solution.

A very interesting and unique nanocomposite structure of PG 0.1wt% can be observed using SEM. As seen above the typical “cauliflower” like structure is not seen as pronounced as observed in the PPy control film sample. On the contrary it is seen a very unique hybrid layered nanostructure is fabricated upon the inclusion of graphene. It can be clearly observed that few individual layers of graphene have been coated with the

polymerized PPy film making it a stacked hybrid structure. The thickness of each and individual layers of these stacks of graphene coated with PPy are approximately 20nm. The distance between two layers is in the range of 300-500 nm suggesting macroporous materials formation (pore size = 50-1000nm).



*Figure 5-8: High resolution SEM micrograph of PPy-graphene (PG 0.1 wt %) concentration at different magnification showing a very unique nanocomposite structure.*

### **5.3.6 Polypyrrole-graphene-CNT nanocomposite electrode (PCG)**

It is evident from the *Figure 5-9*, that the PCG nanocomposite also forms a very unique structure with a layered morphology containing graphene and CNTs.



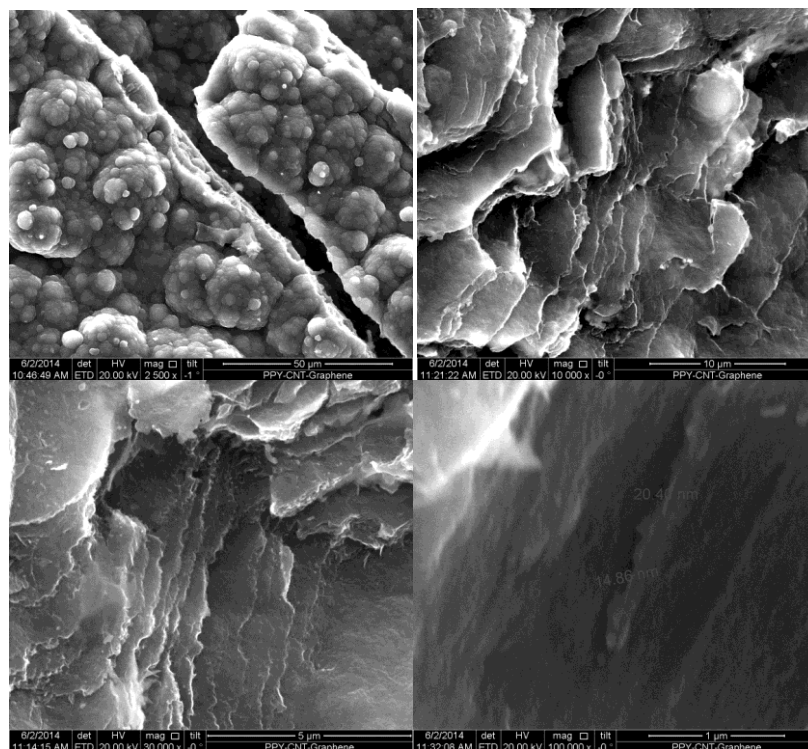


Figure 5-9: SEM micrograph of polypyrrole-graphene-CNT nanocomposite electrode film.

#### 5.4 Energy-dispersive X-ray spectroscopy (EDS)

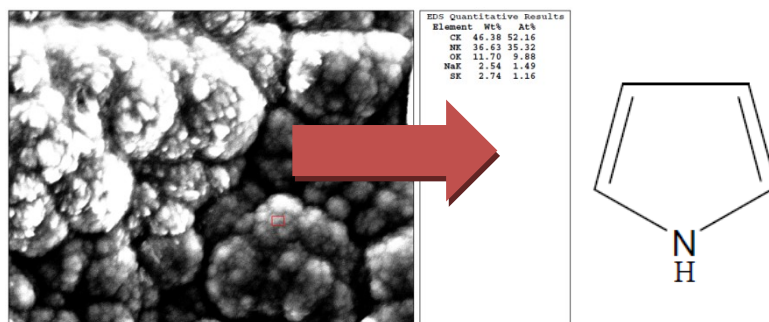


Figure 5-10: Elemental EDS characterization representing the composition of control PPy film before performing the CV.

EDS is very useful technique to analyze the elemental structure of the nanocomposite. This technique relies on an interaction between the sample and some source of X-ray excitation.

## 5.5 Electrochemical Analysis of the nanocomposite electrodes in different electrolytes

Table 5-2: List of the different nanocomposite supercapacitor electrodes with varying concentration of graphene and CNT in the overall pyrrole matrix.

<b>Nanocomposite composition</b>
Polypyrrole control (PPy)
Polypyrrole with 0.01 wt% CNT-graphene (PCG0.01)
Polypyrrole with 0.05 wt% CNT-graphene (PCG0.05)
Polypyrrole with 0.1 wt% CNT-graphene (PCG0.1)

The electrochemical response of control PPy and related nanocomposite was performed using cyclic voltammetry (CV) technique. All the different nanocomposite electrode films were tested using different electrolytes such as sulfuric acid (SA), sodium sulfate (SS) and ascorbic acid (AA) also known as vitamin C. The working electrode (WE) was taken as the PPy and nanocomposite electrodes which is tabulated below.

Using the CV technique initial deposition of the nanocomposite electrodes was performed on the graphite rod where the films of these electrodes were deposited. The deposition took place on the surface of the graphite rod with the diameter of 3mm. The area of all the nanocomposite film was maintained at 7.06858 mm<sup>2</sup>. All the CV tests were performed at different scan rates such as 5, 50, 100 and 500 m V s<sup>-1</sup>.

Table 5-3: Weight of individually deposited nanocomposite freestanding film for electrochemical analysis.

Weight of nanocomposite electrode deposited (mg)	PPy	PCG0.01	PCG0.05	PCG0.1
AA	2	3	2.1	2.8
SS	2	2.3	2.1	2.8
SA	1.6	2.2	1.7	1.5

The weight of the deposited PPy and PCG film was calculated by subtracting the weight of bare graphite electrode with the weight of graphite with deposited film on it. Approximately the total deposited nanocomposite film weighs in the range of 1.5-3 mg as tabulated below.

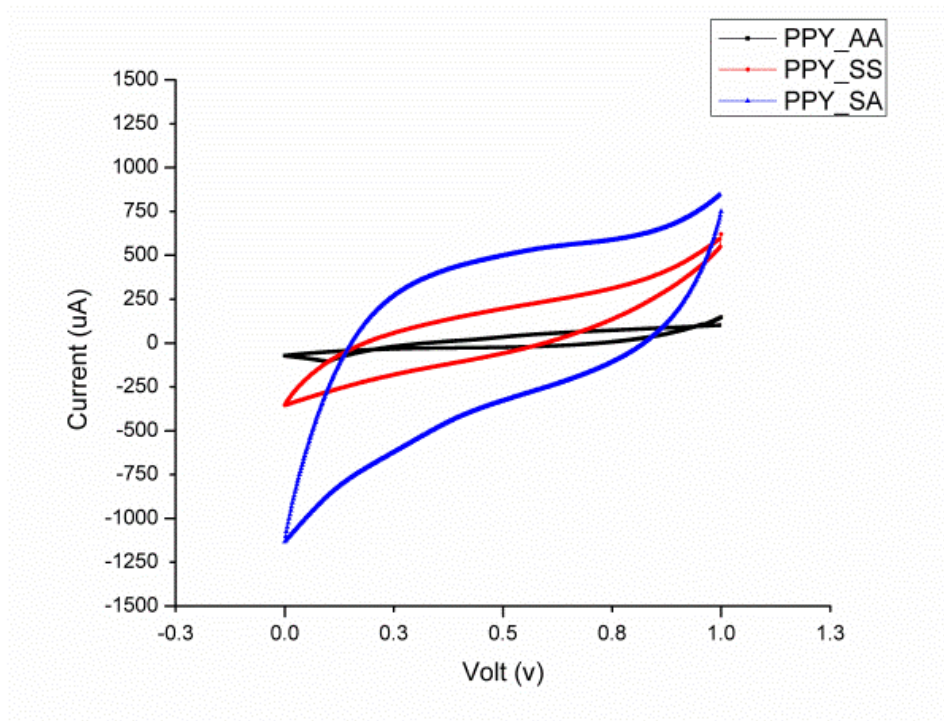


Figure 5-11: Cyclic voltammety comparison of the control PPy nanocomposite in various electrolytes (SA, SS, AA). A typical capacitive curve is obtained by the PPy nanocomposite in SA electrolytes representing higher charge storing capability.

The specific capacitance of the electrodes have been calculated using following:

$$C = \frac{1}{mVs} \int_{V-}^{V+} I(V)dV \quad (5.1)$$

Where  $C$  is the specific capacitance ( $F\ g^{-1}$ ),  $m$  is the mass of the active electrode material (g),  $[V= V_+ -V_-]$  the potential difference and  $s$  is the scan rate ( $m\ V\ s^{-1}$ ). The total charge transferred during the cycle can be calculated by integrating the area under the curve of CV.

Table 5-4: Specific capacitance values of individual nanocomposite films in sulfuric acid (SA) electrolyte as measured by cyclic voltammetry.

Scan rate	PPy control	PCG0.01	PCG0.05	PCG0.1	Sulfuric Acid (SA)
5	281	305	384	453.33	
50	115.5	154	283.33	257.46	
100	90.62	120	156.667	284.66	
500	86	111.355	107.267	69.32	

Table 5-5: Specific capacitance values of individual nanocomposite films in sodium sulfate (SS) electrolyte as measured by cyclic voltammetry.

Scan rate	PPy control	PCG0.01	PCG0.05	PCG0.1	Sodium Sulfate (SS)
5	226.8	264.261	485.9	253.57	
50	116.8	65.42	105.71	37.08	
100	63.2	25	55.62	22	
500	21.04	7	15.9	6.44	

Table 5-6: Specific capacitance values of individual nanocomposite films in ascorbic acid (AA) electrolyte as measured by cyclic voltammetry.

Scan rate	PPy control	PCG0.01	PCG0.05	Ascorbic Acid (AA)
5	219.09	319.165	450.56	
50	104.9	97.645	97.48	
100	38.16	50.581	62.81	
500	24.09	19.69	41.359	

As shown in *Figure 5-12*, it was observed that SA has the highest amount of the specific capacitance which is later followed by the SS and AA electrolytes. This shown that the type of the electrolytes plays a significant role in the charge storage mechanism in the supercapacitor electrodes. This can be better observed in the *Figure 5-13*, where the specific capacitance of the electrodes is calculated from the CV curve in various electrolytes such as SA, SS and AA. In all the electrolytes we observe a common trend of highest amount of specific capacitance with the increase in the concentration of graphene and CNT respectively. This trend suggests that the strong electrolytes which are highly acidic in nature gives rise to higher ion mobility which in turn increases the charge storage capabilities. Also from above images a very obvious trend of increase in the specific capacitance is observed with the decrease in the scan rate. At a very low scan rate the total time for the electrolytic ions to get adsorbed increases drastically hence

allowing more concentration of ions getting in the highly porous structure of the nanocomposite enabling higher amount of specific capacitance.

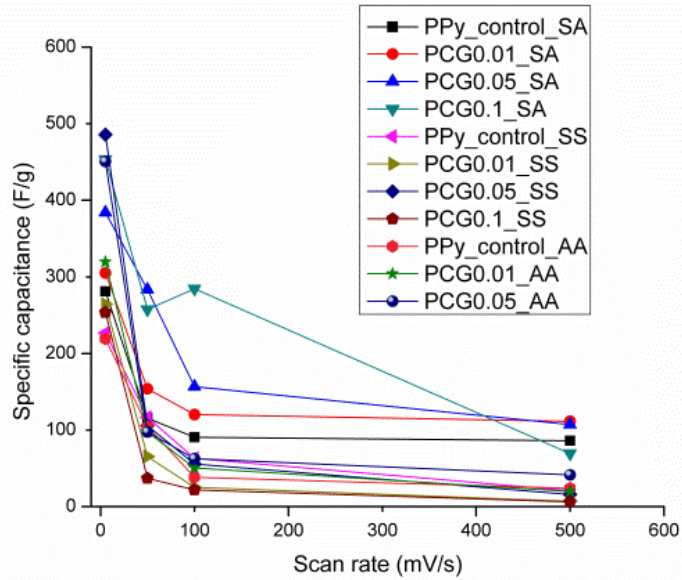


Figure 5-12: Specific capacitance versus the scan rate. Overall observation of higher specific capacitance in SA followed by the SS and least in AA.

Also it can be seen in the case of SA electrolyte that there is a continuous increase in the specific capacitance of the electrodes with the increase in the concentration of graphene and CNT. The control sample of PPy (0 wt %) has the specific capacitance of  $\sim 281 \text{ F g}^{-1}$  at the scan rate of  $5 \text{ m V s}^{-1}$  and it increases with the concentration of PCG to maximum of  $\sim 450 \text{ F g}^{-1}$ . This highly indicates that the unique nanocomposite structure which has been fabricated with the inclusion of graphene and CNT in the polypyrrole matrix plays a significant role in overall charge storage mechanism.

For the PPy control nanocomposite film in H<sub>2</sub>SO<sub>4</sub> electrolyte, the highest capacitance observed was 281 F g<sup>-1</sup> at the scan rate of 5 m V s<sup>-1</sup>. Not only did the H<sub>2</sub>SO<sub>4</sub> electrolyte yield a high capacitance, but also there was a low drop in capacitance as the scan rate increased.

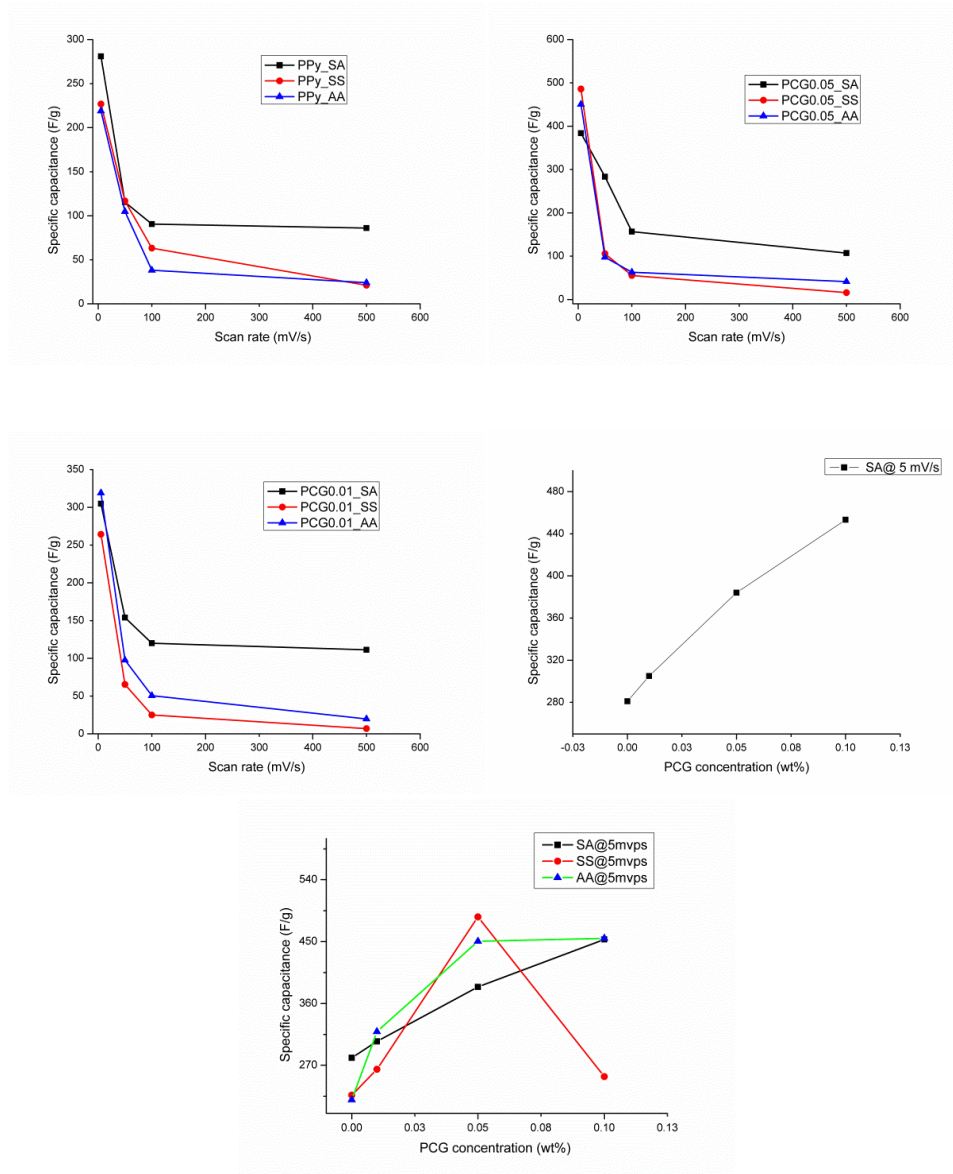
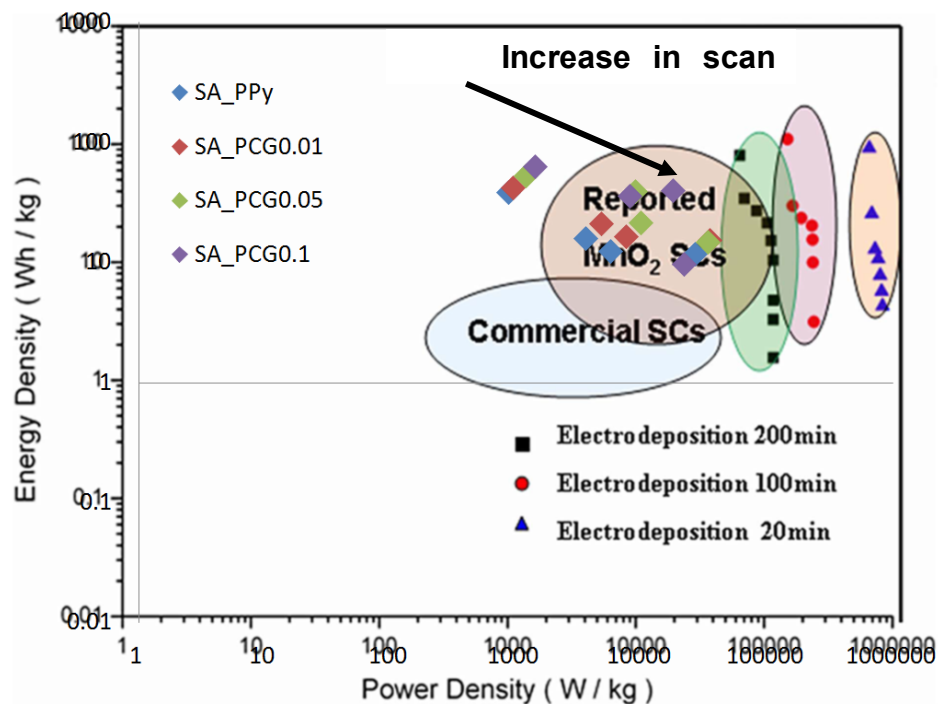


Figure 5-13: Specific capacitance measurements of individual electrodes such as control PPy and different concentrations of PCGs in various electrolytes (SA, SS and AA).



The graph in *Figure 5-13*, displays a consistent trend in the amount of specific capacitance and the type of nanocomposite film. Overall, the PPY film had the lower specific capacitance when compared to the PCG composite films. Furthermore, as the concentration increased for the PCG composite films, the specific capacitance did as well. This trend displays that the higher the concentration of PCG, the higher the specific capacitance.

## 5.6 Power density and Energy density comparison of the electrodes



*Figure 5-14*: A superimposed graph of PCG containing nanocomposite at various scan rates on a Ragone plot which compares the electrodes of supercapacitors from various reference and commercially available supercapacitors. Reproduced from [120], Scientific reports, 2013

Analyzing the cyclic voltammetry curve we can calculate the power density (P, in  $\text{Wkg}^{-1}$ ) and the energy density of the electrode material by using the following expressions

$$P = \frac{1}{mV} \int_0^{V^+} IVdv$$

Here, V is the initial voltage during discharge; m is the total mass of both electrodes

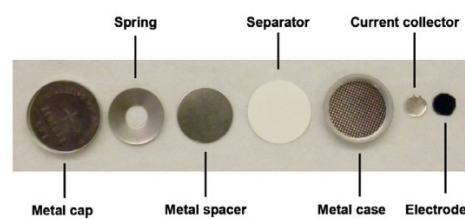
$$E = \frac{1}{3600mv} \int_0^{V^+} IVdv$$

Here  $v$  is the scan rate ( $\text{Vs}^{-1}$ )

Here shown above the specific energy and power density values are very much consistent with the other materials recently reported and the also with various commercial supercapacitors.

## CHAPTER 6. SUPERCAPACITOR DEVICE ASSEMBLY

The supercapacitor test cells were assembled using the CR2032 battery coin cells as shown in the. The test cell consisted of a metal cap, a metal case with the polymer seal, a spring, two stainless steel spacers, two current collectors coated with the active conductive materials and a membrane separator. The capacitor stack of electrodes and separator was positioned between two spacers. Two symmetric conductive electrodes were electrically separated by a hydrophilic membrane which is uniquely made from polycaprolactone (PCL) nanofibers having extremely small diameter and very high specific surface area. This separator membrane was soaked with SA electrolyte acting as electrolyte reservoir as well as it permits the ionic exchange across the two electrodes.



### Actual

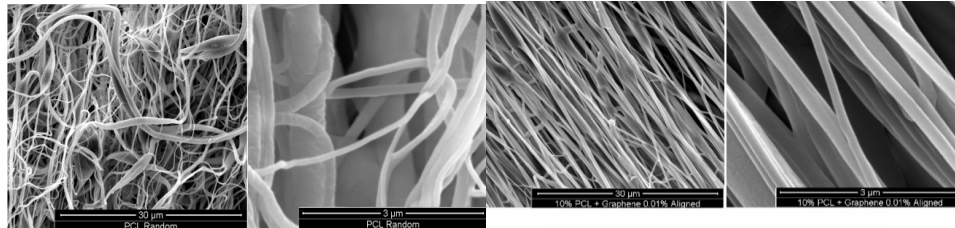
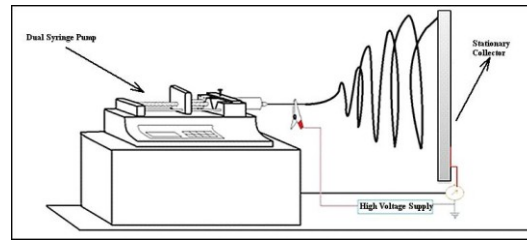


*Figure 6-1:* Supercapacitor test assembly cell device. Left image adapted from [121], image on the right is of the actual supercapacitor device.

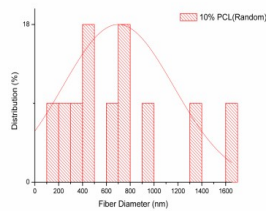
## 6.1 Fabrication of PCL based nanofibrous separator membrane

The electrospinning setup comprised of a dual syringe pump (KDS 200 series, KDS scientific), a high voltage power supply (Model ES30P, Gamma High Voltage Research) and a metallic (aluminum) collector placed at an appropriate distance from the tip of the needle. The variables that are important in electrospinning of nanofibers are, the distance between the needle and the collector ( $d$ ), viscosity of the polymer solution, flow rate ( $r$ ) of the polymer solution from the needle tip through the syringe and electric field strength applied which is voltage per distance (kV/cm) between the needle and the collector.

A



B



C

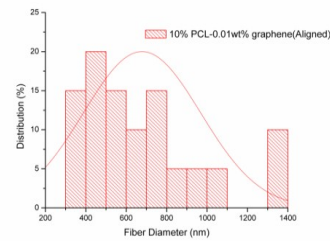


Figure 6-2: A) Typical electrospinning setup having high voltage power supply and syringe pump, B) SEM image of the PCL nanofibers showing nanofibrous structure with average diameter in the range of 600 nm, C) SEM image of electrospun nanofibers completely oriented in one direction using rotating collector.

10 wt% PCL solutions (Sigma Aldrich, 70k-90k Mw) was prepared using 10g of PCL pellets in 100ml acetone solvent and stirring at 60°C until a clear solution was achieved. Polymeric nanocomposite solution was also prepared by adding different concentrations of graphene in 10 wt% PCL solutions. Scanning electron microscope (SEM) was utilized to characterize the morphology of the fibers after sputter coating (CRC 50 Sputter Coater) gold on the sample for 25s.

### 6.1.1 Model for formation of aligned nanofibers on the rotating collector

Understanding of the fiber formation from a single drop of polymeric solution is a non-trivial event. The fundamental equations for fiber formation in melt spinning and various strategies used for alignment of nanofibers in the past few years can be used to understand coaxial alignment of fibers using axially rotating collector (ARC) collector. A mathematical model for alignment of nanofibers on ARC collector using the approximations discussed previously (A.Ziabicki, 1976) and comparing the theory of fiber alignment on rotating drum collector [122], [123].

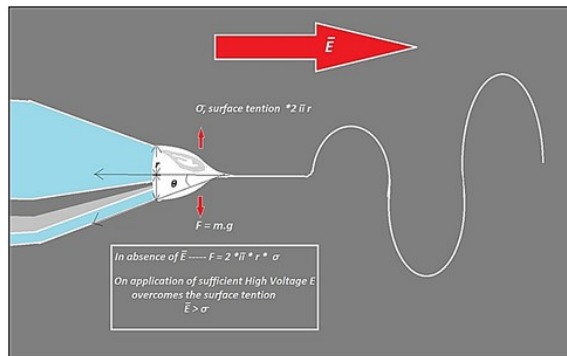


Figure 6-3: Schematic showing various forces acting on a polymer drop at the tip of needle leading to subsequent stretching

As shown in *Figure 6-3*, neglecting gravitational force “F” acting on the drop, the surface tension ‘ $\sigma$ ’ is compensated by force of electric potential across the needle and collector. The droplet is deformed by electric field into conical shape subsequently emerging out as a jet. At this point electric field overcomes the surface tension of the drop.

### 6.1.1.1 Interaction of Tensile Force Introduced By Rotating Disc

The tension force produced by the rotating disc collector ( $F_{rd}$ ) and the force due to gravity ( $F_{gr}$ ) are balanced by the rheological force ( $\sigma$ ) which arises due to the friction between polymer molecules, the aerodynamic force ( $F_{ar}$ ) which is drag exerted by the air flow in the chamber on the fiber jet, the inertial force ( $F_{ir}$ ) and the surface tension of fiber jet ( $\sigma_s$ ).  $F_{ir}$  is a combination of radial forces on charge (R) and cohesive forces among charges (C).

$$F_{rd} + F_{gr} = \sigma + F_{ar} + F_{ir} + \sigma_s \quad (6.1)$$

Above model is important for stability of fiber jet formation[122].

Force on a given point on the rotating disc will be centripetal force exerted on that point during rotation in circular path and can be written as,

$$F_{rd} = ma_c = \frac{m_t V_t^2}{r} \quad (6.2)$$

An axial stress generated in the fiber jet is given by equation

$$\sigma = 3\mu \left( \frac{v_t - v_f}{l} \right) \quad (6.3) \quad [124], [125]$$

Since, fiber jet is subjected to the force of electric field, the surface tension build up in fiber along its cross sectional area will be

$$\sigma_s = \frac{E}{A} \quad (6.4)$$

Gravitational force acting on the fiber jet of mass  $m$ ,

$$F_{gr} = m_f g \quad (6.5)$$

Considering a fiber loops in the median region of setup, equation (6.1) will govern the generation of tensile force in fiber jet and loops. As the fiber loop comes in the nearest region of the collector, the force of rotation of the collector will take up a charge and will generate significant tensile force by the cooperation of electric field strength. Fiber will now deposit starting from its tip, gradually sticking its lateral surface along the circumference of collector. At this point the radius of fiber loop will be stabilized since collector will strongly attract charges within the fiber. Difference between collector velocity ( $V_t$ ) and fiber velocity ( $V_f$ ) will gradually decrease and may approximately be zero. We can assume  $\mu$  to be constant at the time of deposition. Considering no further elongation at this point we can make area of cross section ( $A$ ), length ( $l$ ), and volume ( $V$ ) of a depositing fiber to be constant. Hence we get

$$v_t^2 + r \propto E \quad (6.6)$$

Equation (6) can be used to explain the phenomenon of normalized fiber deposition as,

1) The direct proportionality between collector velocity  $V_t$  and Electric field strength  $E$  shows that  $V_t$  will cooperate with  $E$  to add up a force to maintain the constant orientation of fiber.

2)  $r$  indicates that the fiber loop will now keep on depositing along the radius of the collector. In this case loop radius can be treated as a *Vector quantity*  $\vec{r}$ , being affected by collector velocity ( $V_t$ ) and electric field (E) in the space.

3) The interaction between the electric field and the charge in a polymer jet (fiber) turns the fiber in erratic loops, randomly depositing it on the stationary collector. In order to align fiber coaxially along its circumference, the circular collector should rotate with sufficient rpm high enough and having diameter (radius) large enough to be proportionate to the electric field in the space.

If we consider an electric field E and elongation viscosity  $\mu$  to be constant at the point of deposition, radius to be unaffected, and considerable change in fiber velocity then the equation (6.6) will be,

$$v_t^2 \propto v_t - v_f \quad (6.7)$$

$$\text{Or} \quad v_t^2 - v_t \propto -v_f \quad (6.8)$$

$$\text{Or} \quad v_t(v_t - 1) \propto -v_f \quad (6.9)$$

Negative sign indicates  $v_f < v_t$

Above equation explains that collector velocity will be imparted to the fiber velocity and bring it up to the speed of collector rotation for normalized deposition. In case of  $V_t < V_f$ , the equation (6.7) will be

$$v_t^2 \propto v_f - v_t \quad (6.10)$$

$$\text{i.e.,} \quad v_t(v_t + 1) \propto v_f \quad (6.11)$$

Equation (6.11) is still the as equation (6.9) but its positive sign indicates that it is not significantly affected by the collector velocity and therefore factors like elongation



viscosity, inertial forces may remain in effect up to appreciable extent. At this point, fiber orientation may vary and wouldn't be depositing itself along the circumference. For instance we will take Equation (6.6) in consideration assuming that  $(v_t - v_f)$  is appreciable quantity as

$$v_t^2 + r \propto (v_t - v_f) + E \quad (6.12)$$

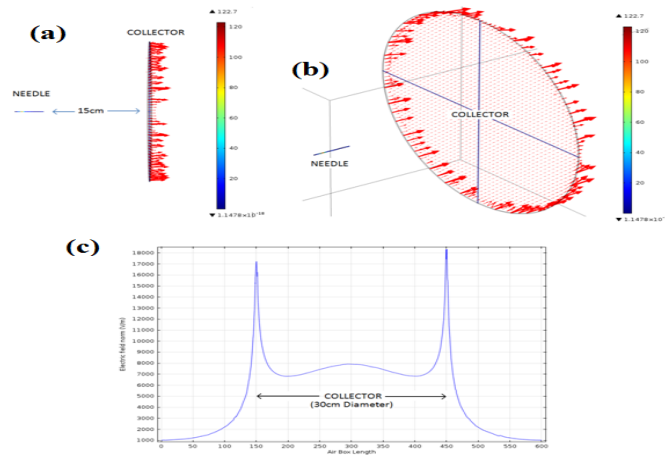
$$\text{Or } v_t^2 + r \propto \Delta V + E \quad (6.13)$$

Where,  $\Delta V = (v_t - v_f)$ ,  $v_t$  will affect the radius of fiber loop and proportionally maintain fiber velocity  $v_f$  or  $\Delta V$ . Because of this over all interaction fiber loop will be acted upon by proportional amount of electric field strength. The entire interaction will result in the phenomenon of normalized deposition.

### 6.1.2 Finite Element based simulation model

A computer simulation model was studied for the syringe and the disc collector in order to understand the electric field patterns that are generated in the surrounding medium (air) between the needle and the collector during the electrospinning of the nanofibers. *Figure 6-4* shows the electric field in the form of an isosurface, where we can clearly see the electric field lines targeting the grounded aluminum collector at its periphery. The needle is modeled as a high-strength alloy steel cylinder with 40 mm length and 0.8 mm diameter. Similarly, the aluminum disc collector is modeled as a 300 mm diameter disc having a thickness of 1mm. Material properties are assigned as per standard values for relative permittivity and electric conductivity for the needle, disc and the surrounding air. It is known that air is a very good insulator, however, at high voltages such as in case of electrospinning (~15 kV), the medium between the needle and

the collector ionizes thereby slightly increasing the conductivity and hence to accommodate this aspect, an initial electric conductivity of  $1 \times 10^{-14}$  S/m for air is considered. Furthermore, a tetrahedral meshing algorithm was used for finite element analysis and 3D as well as 2D plot groups in COMSOL multiphysics were utilized for the analysis of the resulting electric field. It was found that the aluminum collector is primarily impacted at its periphery by the emanating electric field lines from the needle tip at 15kV (Figure 6-4 (A) and (B)). It was realized that the accumulation of nanofibers would be higher at the periphery mainly due to this effect.



*Figure 6-4:* Electric Field modeling and analysis showing the electric field pattern at the collector surface. (a) Distance between the needle (positive terminal) and the collector (ground) showing the electric field lines. The length and thickness of the arrows is proportional to the intensity of the field (maximum of 122.7 V/m), (b) a 3-D view of the model showing the electric field predominantly over the periphery of the disc collector anticipating a larger accumulation of nanofibers over the periphery, (c) line graph plot showing the highest intensity of the electric field at the periphery of the 30cm diameter collector. The difference in field strength ( $\sim 1000$  V/m) between the two edges is due to the error in positioning the arc across the disc collector

The resultant plot of electric field (V/m) with respect to the arc length across the disc in the y-z plane demonstrated that there is a significant difference in the electric field intensity at the periphery compared to the disc ( $\sim 10,000$  V/m). The little difference in the

electric field between the two peripheral sides of the disc is due to a slight mismatch in the two ends of the arc length across the air box.

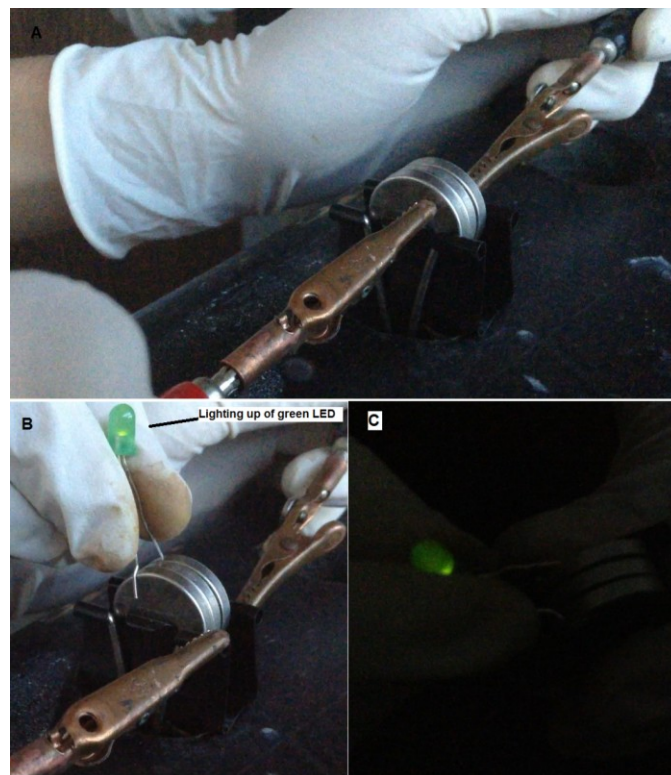
## 6.2 Electrical measurements of the supercapacitor device

The supercapacitor stack was fabricated as shown in the Figure 6-5 which is described in detail in the section 0. In order to compare the performance of the supercapacitor device, the voltage comparison was done of conventional alkaline 1.5 V battery and stacks of supercapacitor as shown in Figure 6-5.



Figure 6-5: A) Supercapacitor device assembled and ready to be tested. B) Measurement of the output voltage from a conventional alkaline 1.5 V battery, C) Output voltage of supercapacitors stacked in three cells made from CR2032 stainless steel coins. The overall output voltage of the device is approximately 1.5 V

The output voltage of the conventional alkaline battery is 1.5 V and that of the assembled stacks of supercapacitor devices together is 1.5 V prior to charging of the supercapacitor cells. These supercapacitor cells were charged using a power supply of 5V/ 3A for only 10 s after which the device voltage was ramped up to  $\sim 2.5$  V. This demonstrates supercapacitor capability to be charged only in few seconds as compared to minutes or hours in the case of the conventional batteries. This also suggests the high performance of the stacks of supercapacitor using the nanostructures electrode material which has very minimal weight as compared to the conventional battery which densely packed with toxic electrode materials.

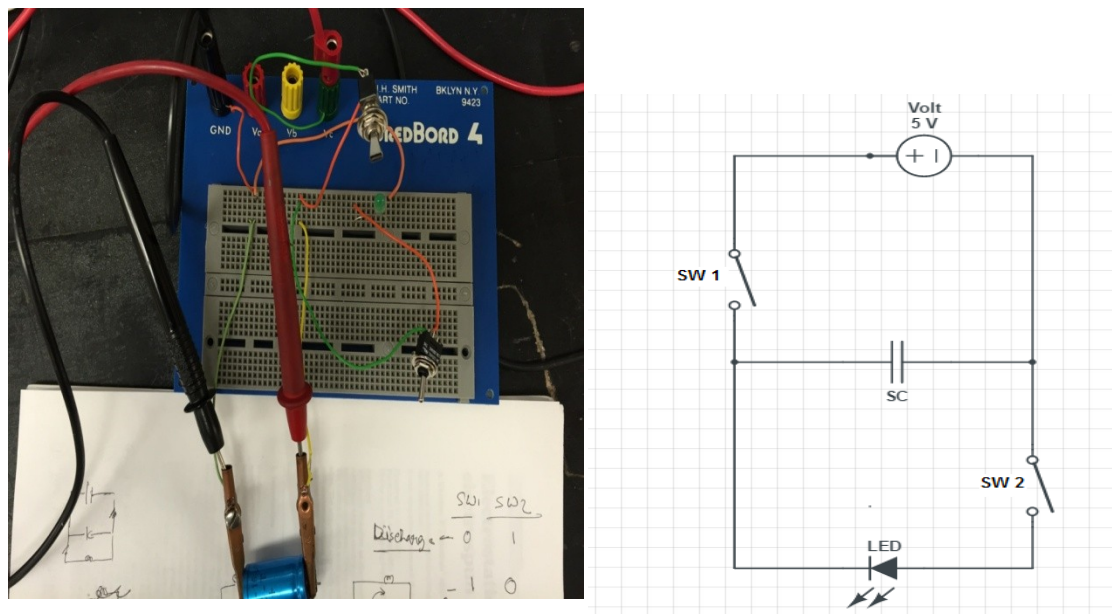


*Figure 6-6:* A) Charging of the supercapacitor device using external power supply with constant 5V / 3A. The supercapacitor device needs to be charged only for 10 s giving the output voltage of  $\sim 2.5$  V. B & C) Demonstrates the lighting up of green LED (2.2V) using the supercapacitor device after charging.

Further to demonstrate the actual operation of the supercapacitor device, a green LED was used in series connected to the positive and negative terminals of the supercapacitor device as shown in *Figure 6-6*. The supercapacitor device was charged using external power supply for 10 s and the output voltage was ramped up to 2.5V from 1.5 V. After this a 2.2 V green LED bulb was connected to the supercapacitor device which was able to light up. This demonstrates that ionic charges stored in the supercapacitor device while charging were utilized to light up a bulb.

### 6.2.1 Circuit Implementation

To further demonstrate the performance of the supercapacitor stack a sophisticated circuit was implemented using 2 switches as shown in *Figure 6-7*.



*Figure 6-7:* A) Experimental circuit implementation for demonstration of supercapacitor performance, B) Circuit diagram illustrating the same circuit design.

Here as show above two switches are used across the stack of supercapacitors. SW1 connects the power source to the supercapacitor and charges it for 30 s. SW2 when turned ON connects the supercapacitors to the LED and discharges emitting the light. Using this circuit a thorough comparison has been done using conventional capacitors and the fabricated supercapacitors. Table 6-1 demonstrates the test cases for the implemented circuit.

Table 6-1: Test cases for the implemented circuit

Case	SW 1	SW 2	SC (charging/discharging)
1	0	0	Not charging
2	1	0	Charging
3	0	1	Discharging to load (LED)

It is observed that the conventional supercapacitor would charge in few milliseconds however it would light up the LED for only few milliseconds. On the contrary to this a supercapacitor stack would take about 30 s to charge up to 3 V and it would light up the LED for a good 3 min indicating the power and energy density of these nanostructured electrodes and their capability to store the charges for a longer period of time.

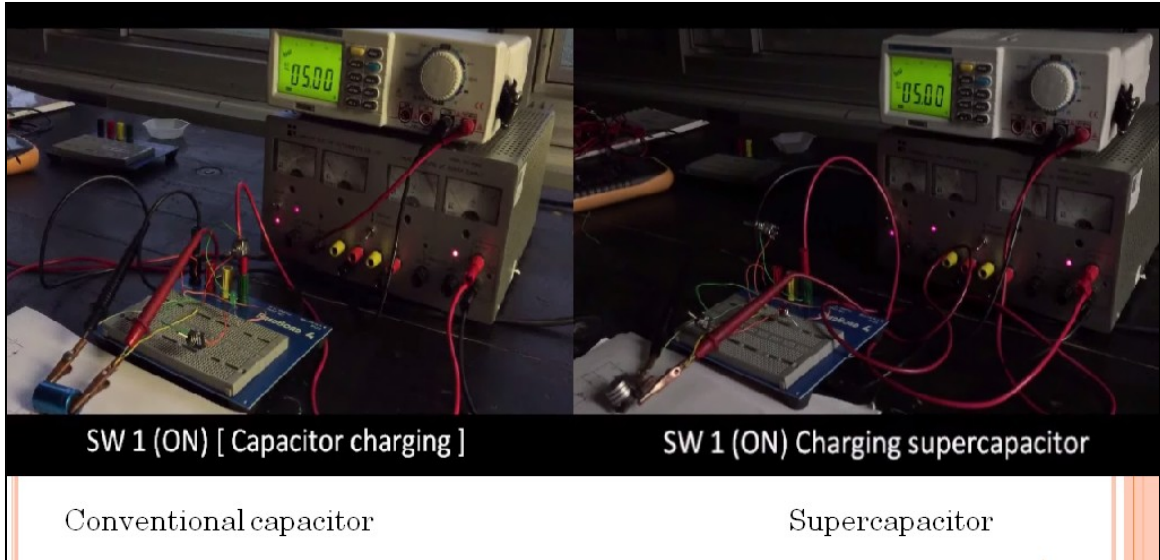


Figure 6-8: Comparison of a conventional capacitor with stacks of supercapacitor using the implemented circuit.

A supercapacitor device self discharge performance was also done as shown in the Figure 6-9.

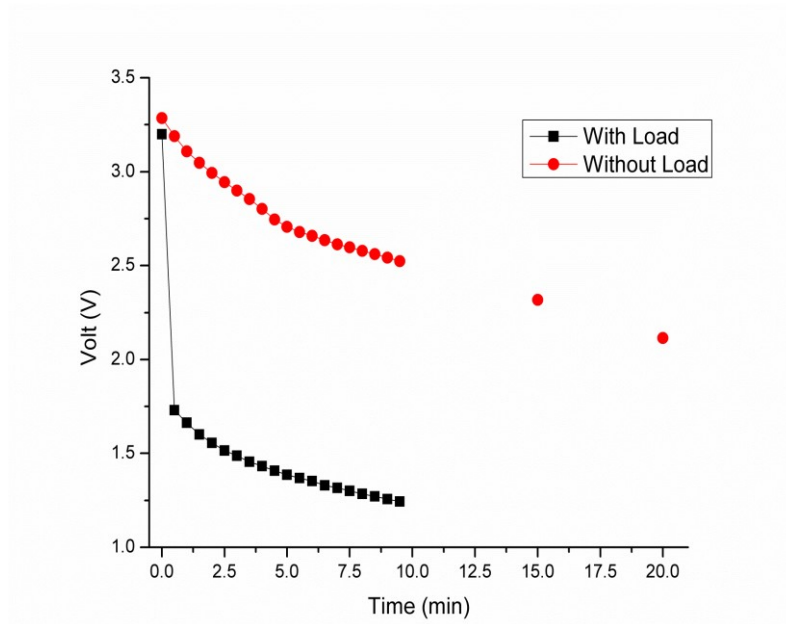


Figure 6-9: Discharge profile of the supercapacitor stack with and without the presence of load (LED) with respect to time (min)

## CHAPTER 7. APPLICATION SPECIFIC MODELING OF THE SUPERCAPACITOR

### 7.1 Mathematical model for theoretical specific capacitance of the polypyrrole electrode in sulfuric acid

The performance of the supercapacitor device of PPy and PCG nanocomposite was characterized using cyclic voltammetry. For the CV method, the overall specific capacitance can be obtained from,

$$C = \frac{dq}{dE} = \frac{dq}{dt} \frac{dt}{dE} = i \frac{dt}{dE} = \frac{i}{dE/dt} = \frac{i}{v} \quad (7.1)$$

Here,  $i$  (A) is the instantaneous current in the cyclic voltammetry curves,  $dE/dt$  ( $\text{Vs}^{-1}$ ) is the scan rate ( $v$ ,  $\text{Vs}^{-1}$ ) and  $C$  is the capacitance (F) can be calculated by average current ( $i$ ) divided by the scan rate :

$$C = \frac{i}{v} = \frac{1}{(E_2 - E_1)v} \int_{E_1}^{E_2} i(E) dE \quad (7.2)$$

Here  $E_1$  and  $E_2$  are the switching potentials in the cyclic voltammetry,  $\int_{E_1}^{E_2} i(E) dE$  is the voltammetric charge ( $q$ ) obtained by the integration of positive and negative sweep in the CV curves.



The specific capacitance can be calculated by dividing the active mass ( $m$ ) in grams of the electrode to the overall capacitance value.

$$C_{sp} = \frac{C}{m}$$

### 7.1.1 Estimate of maximum value of specific capacitance

Several assumptions need to be made in order to estimate the theoretical value of the nanocomposite electrodes which are as follows [49]:

- 1) The polypyrrole nanocomposite film is solid and the entire surface is applied in charge storage mechanism
- 2) The diffusion process of the counter- anions ( $\text{SO}_4^{-1}$ ) is fast enough and has no effect on the faradaic reaction of PPy
- 3) The PPy film has high conductivity under various conditions

Based on the assumptions it can be considered that the redox reaction takes place in the PPy film instantaneously at the same time everywhere. The redox potential of the PPy film is  $E_{pa} = 0.45 \text{ V}$  and  $E_{pc} = -0.123 \text{ V}$ , hence  $\Delta E = 0.573 \text{ V}$

Now the charge stored in the PPy nanocomposite due to the faradaic reaction is;

$$Q_p = nF \quad (7.3)$$

Here,  $n$  is the number of moles of repeated units in Py,  $F$  is the Faraday constant,  $9.64853 \times 10^4 \text{ C mol}^{-1}$ . The capacitance can be calculated from  $Q_p$  as:

$$C_p = \frac{Q_p}{\Delta E} \quad (7.4)$$

Here,  $\Delta E$  is the potential window for PPy electrode. Hence the specific capacitance ( $C_{sp}$ ) can be calculated as follows:

$$C_{sp} = \frac{C_p}{m} = \frac{Q_p}{\Delta E \times m} \quad (7.5)$$

Now for PPy the with 1 mole of Pyrrole repeating units, the faradaic charge stored  $Q_p$  is;

$$Q_p = 1 \times 1 \times 9.64853 \times 10^4 = 94685.3 \text{ C} \quad (7.6)$$

The potential window of PPy,  $\Delta E = 0.573 \text{ V}$  and with 1 mole of repeat units of the Py is 67.09 g.

Therefore,

$$C_{sp} = \frac{Q_p}{\Delta E \times m} = \frac{96485.3}{0.573 \times 67.09} = 2509.85 \text{ F/g}$$

Approximately we can consider the specific capacitance of single PPy electrode system as  $2500 \text{ F g}^{-1}$ . Considering this the specific capacitance of a symmetrically stacked supercapacitor will be:

$$\frac{1}{C_{cell}} = \frac{1}{C_1} + \frac{1}{C_2}$$

$$C_{cell} = \frac{C_{sp} \text{ of single electrode}}{2} = \frac{2500}{2} = 1250 \text{ F/g}$$

Hence the theoretical limit of the PPy nanocomposite electrode based supercapacitor would be  $\sim 1250 \text{ F g}^{-1}$ .

## 7.2 Supercapacitor in hybrid electric vehicles (HEV) application

One of the very unique applications of supercapacitors can be thought of using it in hybrid vehicles. The configuration of the hybrid vehicles can be done in several ways keeping in mind the efficiency of the primary fuel to wheel torque. The motive behind introducing supercapacitors in hybrid vehicles is to reduce the overall output stress on the battery pack and also to utilize the peak power requirements in electrical systems.

Table 7-1: Technical data, Toyota Prius, 2008

Mass (m)	1330	Kg
Maximum power of engine $P_{em, \max}$	50	kW
Power for battery, rated ( $P_b$ )	21	kW
Battery volts, $V_{\text{batt}}$	201.60	V

The maximum power available through the electrical drive train systems is only  $\mp$  50kW. Further it is well known that amount of power requirement during acceleration and braking of the car is more than the limited amount available of 50kW. The braking

and acceleration of car typically lasts for 3-5 s and the total energy required during those 3-5 s is approximately 70 Wh. Typically the excessive braking power will be met by the friction brakes, and the ICE and battery will provide the excess energy needed during acceleration.

The total voltage needed by the battery to meet these excessive power requirement is ~201.06 V.

A typical stack of 3 supercapacitor cells provides voltage approximately 2.5V.

The number of such 3 supercapacitors stacked packs needed are:

$$n = \frac{201.06}{2.5} = 80.4$$

Therefore to provide 201.06V of voltage we need 80 such 3 supercapacitor cell packs. Considering the weight and the size factor of these cells it is highly feasible to use 80 such supercapacitors cell packs.

### **7.3 Mathematical model for power backup using supercapacitors to prevent data loss**

Mostly the transit data or data in the volatile memory are compromised in cases of sudden power failure. In order to protect such data many systems uses battery based power backup systems that supplies short term power enough for the RAID controller to write volatile data to nonvolatile memory.

From the sustainability point of view a lots of research is done in order to replace battery based storage systems. Supercapacitors are finding a very unique application in these advanced flash memory storage systems which can last longer with higher performance and environmentally sustainable. Even though supercapacitors have lower energy density as compared to the conventional batteries, the reduce requirements in flash memory have made them a perfect option for memory backup applications

### 7.3.1 Backup power application

A supercapacitor stack can be incorporated in to a backup system that has the capacity to complete the data transfer out of volatile memory. By using the approximations previously discussed by Jim Drew [126] an estimation of the supercapacitor size and the amount of the electrode materials can be made. A DC/DC converter takes the output of the supercapacitor stack and provides a constant voltage to the data recovery electronics [126]. The data transfer must be completed before the voltage across the supercapacitor drops to the minimum input operating voltage ( $V_{uv}$ ) of the DC/DC converter.

The minimum capacitance ( $C_{min}$ ) required by the supercapacitor can be calculated using backup time ( $T_{bu}$ ) to transfer the data into the flash memory. The initial and the final stack voltage ( $V_{c(0)}$ ) and ( $V_{c(uv)}$ ).

$$C_{min} = \frac{2 \times Pin \times Tbu}{Vc(0)^2 - Vc(uv)^2}$$

So the  $C_{min}$  is the effective capacitance of the one supercapacitor.

Considering that it takes approximately 45 s to store the data in flash memory and the input power to the DC/DC converter is 20W and the  $U_{uv}$  is 2.7V

Assume,

The minimum voltage needed on the supercapacitor stack

$$V_c(uv) = V_{uv} \times 1.1$$

$$V_c(uv) = 2.7 \times 1.1 = 2.97 \text{ V} \approx 3 \text{ V}$$

Hence the minimum capacitance required for the supercapacitor stack is:

$$C_{min} = \frac{2 \times P_{in} \times T_{bu}}{V_c(0)^2 - V_c(uv)^2}$$

$$C_{min} = \frac{2 \times 20 \times 45}{4.8^2 - 3^2} = 128 \text{ F}$$

Assuming the average specific capacitance of the electrode in a single capacitor to be  $300 \text{ Fg}^{-1}$ . The specific capacitance of one supercapacitor device can be calculated

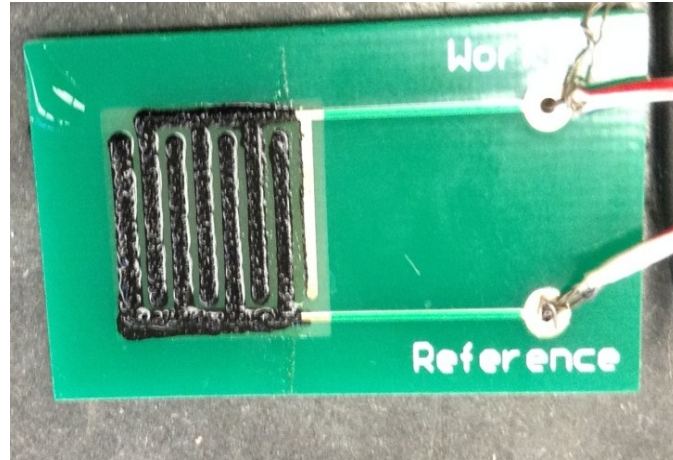
$$\frac{1}{C_{eq}} = \frac{1}{C_1} + \frac{1}{C_2} = \frac{1}{300} + \frac{1}{300} = \frac{2}{300}$$

$$C_{eq} = 150 \text{ F g}^{-1}$$

Hence, should we use about 1 g of nanocomposite materials in one supercapacitor device we can achieve the above required capacitance value.

## 7.4 Microelectrode supercapacitor

Based on the detailed electrochemical characterization of the freestanding electrode film which has shown a very superior performance in terms of the supercapacitor for energy storage application.



*Figure 7-1:* Photograph of a capacitive microelectrode demonstrating the capability of precisely depositing electrically conductive electrode with higher performance.

It can further be shown that these conductive electrode nanocomposite films can be precisely deposited on an existing circuit such as microcomb electrodes as shown in *Figure 7-1*. Using this technique we can precisely pattern the electrical circuit and thereby creating a new opportunity in making flexible circuits.

## CONCLUSIONS

This work demonstrates the use of the sustainable and abundantly available cellulose extracted from *c. aegagropila* algae coated with polypyrrole and graphene as an electrode for supercapacitor application. The nanocomposite was fabricated using *in situ* polymerization of Py monomer mixed with graphene. The introduction of high specific surface area graphene nanoplatelets enables the nanocomposite to achieve high specific capacitance of  $91.5 \text{ Fg}^{-1}$ . The nanocomposite exhibits better electrochemical performance with graphene. Also a novel hybrid nanocomposite has been developed using graphene-carbon nanotubes (CNTs) coated with electrically conductive polypyrrole (PPy). The nanocomposite fabricated by electropolymerization technique was used as an electrode for a supercapacitor device. The electrodes were tested in various electrolytes such as ascorbic acid, sodium sulfate and sulfuric acid. It is found that sulfuric acid electrolyte gave consistently higher specific capacitance in all the scan rates. The specific capacitance of polypyrrole-graphene-CNT nanocomposite as calculated from cyclic voltammetry curve is  $450 \text{ Fg}^{-1}$  at the scan rate  $5 \text{ mVs}^{-1}$  with highest concentration of graphene-CNT of 0.1 wt%. The power density and energy density of these electrodes is compared in Ragone plot with existing commercial supercapacitors and various supercapacitors electrodes reported by other research groups. A unique highly porous nanofibrous scaffold has been fabricated using electrospinning setup which was used as a separator which acts as electrolyte reservoir and as ionic exchange membrane. It was observed that due to extremely high specific surface area of these nanostructured fibers the ionic diffusion happens extremely efficient giving rise to higher charge storage



capabilities. A thorough morphological and electrochemical characterization has been performed to achieve fundamental understanding of these electrodes. Mathematical model predicting the theoretical limit of the polypyrrole nanocomposite has been proposed. The performance of the fabricated supercapacitor device has been analyzed using a multimeter and compared with a conventional alkaline (1.5V) battery and a conventional capacitor. Lighting up of 2.2 V light emitting diode has been demonstrated using the fabricated supercapacitor. Application specific modeling has also been introduced. These applications include the use of the fabricated supercapacitor in hybrid electric vehicles (HEV), power back-up in memory storage and as microelectrodes in flexible electronics. A fundamental understanding of the advanced supercapacitor have been achieved through carefully designed experiments and characterizing the nanocomposite using some of the state-of-the-art techniques.

## REFERENCES

- [1] P. Simon and Y. Gogotsi, "Materials for electrochemical capacitors," *Nat Mater*, vol. 7, no. 11, pp. 845–854, Nov. 2008.
- [2] M. D. Stoller, S. Park, Y. Zhu, J. An, and R. S. Ruoff, "Graphene-based ultracapacitors.," *Nano Lett.*, vol. 8, no. 10, pp. 3498–502, Oct. 2008.
- [3] X. Yu, B. Lu, and Z. Xu, "Super Long-Life Supercapacitors Based on the Construction of Nanohoneycomb-Like Strongly Coupled CoMoO<sub>4</sub> -3D Graphene Hybrid Electrodes.," *Adv. Mater.*, vol. 26, no. 7, pp. 1044–51, Feb. 2014.
- [4] C. Portet, P. L. Taberna, P. Simon, E. Flahaut, and C. Laberty-Robert, "High power density electrodes for Carbon supercapacitor applications," *Electrochim. Acta*, vol. 50, no. 20, pp. 4174–4181, Jul. 2005.
- [5] E. Karden, S. Ploumen, B. Fricke, T. Miller, and K. Snyder, "Energy storage devices for future hybrid electric vehicles," *J. Power Sources*, vol. 168, no. 1, pp. 2–11, May 2007.
- [6] L. Oakes, A. Westover, J. W. Mares, S. Chatterjee, W. R. Erwin, R. Bardhan, S. M. Weiss, and C. L. Pint, "Surface engineered porous silicon for stable, high performance electrochemical supercapacitors.," *Sci. Rep.*, vol. 3, p. 3020, Jan. 2013.
- [7] H. Yang, S. Kannappan, A. S. Pandian, J.-H. Jang, Y. S. Lee, and W. Lu, "Achieving Both High Power and Energy Density in Electrochemical Supercapacitors with Nanoporous Graphene Materials," Nov. 2013.
- [8] J. Chmiola, G. Yushin, R. Dash, and Y. Gogotsi, "Effect of pore size and surface area of carbide derived carbons on specific capacitance," *J. Power Sources*, vol. 158, no. 1, pp. 765–772, Jul. 2006.
- [9] Y.-C. Chen, Y.-K. Hsu, Y.-G. Lin, Y.-K. Lin, Y.-Y. Horng, L.-C. Chen, and K.-H. Chen, "Highly flexible supercapacitors with manganese oxide nanosheet/carbon cloth electrode," *Electrochim. Acta*, vol. 56, no. 20, pp. 7124–7130, Aug. 2011.

- [10] K. H. An, K. K. Jeon, J. K. Heo, S. C. Lim, D. J. Bae, and Y. H. Lee, "High-Capacitance Supercapacitor Using a Nanocomposite Electrode of Single-Walled Carbon Nanotube and Polypyrrole," *J. Electrochem. Soc.*, vol. 149, no. 8, p. A1058, Aug. 2002.
- [11] D. Pech, M. Brunet, H. Durou, P. Huang, V. Mochalin, Y. Gogotsi, P.-L. Taberna, and P. Simon, "Ultrahigh-power micrometre-sized supercapacitors based on onion-like carbon.," *Nat. Nanotechnol.*, vol. 5, no. 9, pp. 651–4, Sep. 2010.
- [12] A. Izadi-Najafabadi, T. Yamada, D. N. Futaba, M. Yudasaka, H. Takagi, H. Hatori, S. Iijima, and K. Hata, "High-power supercapacitor electrodes from single-walled carbon nanohorn/nanotube composite.," *ACS Nano*, vol. 5, no. 2, pp. 811–9, Feb. 2011.
- [13] J. Tao, N. Liu, W. Ma, L. Ding, L. Li, J. Su, and Y. Gao, "Solid-state high performance flexible supercapacitors based on polypyrrole-MnO<sub>2</sub>-carbon fiber hybrid structure.," *Sci. Rep.*, vol. 3, p. 2286, Jan. 2013.
- [14] Y. S. Lim, Y. P. Tan, H. N. Lim, W. T. Tan, M. A. Mahnaz, Z. A. Talib, N. M. Huang, A. Kassim, and M. A. Yarmo, "Polypyrrole/graphene composite films synthesized via potentiostatic deposition," *J. Appl. Polym. Sci.*, p. n/a–n/a, 2012.
- [15] X. Peng, K. Huo, J. Fu, X. Zhang, B. Gao, and P. K. Chu, "Coaxial PANI/TiN/PANI nanotube arrays for high-performance supercapacitor electrodes.," *Chem. Commun. (Camb)*, vol. 49, no. 86, pp. 10172–4, Oct. 2013.
- [16] L. Wang, Y. Ye, X. Lu, Z. Wen, Z. Li, H. Hou, and Y. Song, "Hierarchical nanocomposites of polyaniline nanowire arrays on reduced graphene oxide sheets for supercapacitors.," *Sci. Rep.*, vol. 3, p. 3568, Jan. 2013.
- [17] H. Lin, L. Li, J. Ren, Z. Cai, L. Qiu, Z. Yang, and H. Peng, "Conducting polymer composite film incorporated with aligned carbon nanotubes for transparent, flexible and efficient supercapacitor.," *Sci. Rep.*, vol. 3, p. 1353, Jan. 2013.
- [18] A. Laforgue, P. Simon, J. F. Fauvarque, M. Mastragostino, F. Soavi, J. F. Sarrau, P. Lailier, M. Conte, E. Rossi, and S. Saguatti, "Activated Carbon/Conducting Polymer Hybrid Supercapacitors," *J. Electrochem. Soc.*, vol. 150, no. 5, p. A645, May 2003.
- [19] H. Ji, X. Zhao, Z. Qiao, J. Jung, Y. Zhu, Y. Lu, L. L. Zhang, A. H. MacDonald, and R. S. Ruoff, "Capacitance of carbon-based electrical double-layer capacitors.," *Nat. Commun.*, vol. 5, p. 3317, Jan. 2014.

- [20] T. Ohta, A. Bostwick, T. Seyller, K. Horn, and E. Rotenberg, “Controlling the electronic structure of bilayer graphene,” *Science*, vol. 313, no. 5789, pp. 951–4, Aug. 2006.
- [21] a K. Geim and K. S. Novoselov, “The rise of graphene,” *Nat. Mater.*, vol. 6, no. 3, pp. 183–91, Mar. 2007.
- [22] A. H. Castro Neto, N. M. R. Peres, K. S. Novoselov, and A. K. Geim, “The electronic properties of graphene,” *Rev. Mod. Phys.*, vol. 81, no. 1, pp. 109–162, Jan. 2009.
- [23] C. C. D. US EPA, “U.S. Greenhouse Gas Inventory Report.” .
- [24] D. Lindley, “Smart grids: The energy storage problem,” *Nature*, vol. 463, no. 7277, pp. 18–20, Jan. 2010.
- [25] Q. Schiermeier, J. Tollefson, T. Scully, A. Witze, and O. Morton, “Energy alternatives: Electricity without carbon,” *Nature*, vol. 454, no. 7206, pp. 816–23, Aug. 2008.
- [26] W. U. Huynh, J. J. Dittmer, and A. P. Alivisatos, “Hybrid nanorod-polymer solar cells,” *Science*, vol. 295, no. 5564, pp. 2425–7, Mar. 2002.
- [27] C. J. Brabec, N. S. Sariciftci, and J. C. Hummelen, “Plastic Solar Cells,” *Adv. Funct. Mater.*, vol. 11, no. 1, pp. 15–26, Feb. 2001.
- [28] B. C. Steele and A. Heinzl, “Materials for fuel-cell technologies,” *Nature*, vol. 414, no. 6861, pp. 345–52, Nov. 2001.
- [29] J. M. Tarascon and M. Armand, “Issues and challenges facing rechargeable lithium batteries,” *Nature*, vol. 414, no. 6861, pp. 359–67, Nov. 2001.
- [30] P. Poizot, S. Laruelle, S. Grugeon, L. Dupont, and J. M. Tarascon, “Nano-sized transition-metal oxides as negative-electrode materials for lithium-ion batteries,” *Nature*, vol. 407, no. 6803, pp. 496–9, Sep. 2000.
- [31] A. S. Aricò, P. Bruce, B. Scrosati, J.-M. Tarascon, and W. van Schalkwijk, “Nanostructured materials for advanced energy conversion and storage devices,” *Nat. Mater.*, vol. 4, no. 5, pp. 366–77, May 2005.
- [32] R. Kötz and M. Carlen, “Principles and applications of electrochemical capacitors,” *Electrochim. Acta*, vol. 45, no. 15–16, pp. 2483–2498, May 2000.
- [33] H. Ibrahim, A. Ilinca, and J. Perron, “Energy storage systems--Characteristics and comparisons,” *Renew. Sustain. Energy Rev.*, vol. 12, no. 5, pp. 1221–1250, 2008.

- [34] S. Vazquez, S. M. Lukic, E. Galvan, L. G. Franquelo, and J. M. Carrasco, "Energy Storage Systems for Transport and Grid Applications," *IEEE Trans. Ind. Electron.*, vol. 57, no. 12, pp. 3881–3895, Dec. 2010.
- [35] L. Ma and Y. Yang, "Solid-state supercapacitors for electronic device applications," *Appl. Phys. Lett.*, vol. 87, no. 12, p. 123503, Sep. 2005.
- [36] L. Ma, J. Ouyang, and Y. Yang, "High-speed and high-current density C[<sub>sub 60</sub>] diodes," *Appl. Phys. Lett.*, vol. 84, no. 23, p. 4786, Jun. 2004.
- [37] J. H. Burroughes, D. D. C. Bradley, A. R. Brown, R. N. Marks, K. Mackay, R. H. Friend, P. L. Burns, and A. B. Holmes, "Light-emitting diodes based on conjugated polymers," *Nature*, vol. 347, no. 6293, pp. 539–541, Oct. 1990.
- [38] L. Ma, Q. Xu, and Y. Yang, "Organic nonvolatile memory by controlling the dynamic copper-ion concentration within organic layer," *Appl. Phys. Lett.*, vol. 84, no. 24, p. 4908, May 2004.
- [39] L. Ma, J. Liu, S. Pyo, Q. Xu, and Y. Yang, "Organic Bistable Devices," *Mol. Cryst. Liq. Cryst.*, vol. 378, no. 1, pp. 185–192, Jan. 2002.
- [40] L. Ma and Y. Yang, "Unique architecture and concept for high-performance organic transistors," *Appl. Phys. Lett.*, vol. 85, no. 21, p. 5084, Nov. 2004.
- [41] N. P. Myhrvold and K. Caldeira, "Greenhouse gases, climate change and the transition from coal to low-carbon electricity," *Environ. Res. Lett.*, vol. 7, no. 1, p. 014019, Mar. 2012.
- [42] P. Simon and Y. Gogotsi, "Charge storage mechanism in nanoporous carbons and its consequence for electrical double layer capacitors," *Philos. Trans. A. Math. Phys. Eng. Sci.*, vol. 368, no. 1923, pp. 3457–67, Jul. 2010.
- [43] H. I. Becker, "US2800616 A," 1957.
- [44] M. Endo, T. Takeda, Y. Kim, K. Koshiba, and K. Ishii, "High Power Electric Double Layer Capacitor (EDLC's); from Operating Principle to Pore Size Control in Advanced Activated Carbons," *Carbon Sci.*, vol. 1, no. 3&4, pp. 117–128, 2001.
- [45] F. Benguin and E. Frackowiak, "Carbons for Electrochemical Energy Storage and Conversion Systems," *CRC Press book*, 2009. [Online]. Available: <http://www.crcpress.com/product/isbn/9781420053074>. [Accessed: 11-May-2014].
- [46] A. G. Pandolfo and A. F. Hollenkamp, "Carbon properties and their role in supercapacitors," *J. Power Sources*, vol. 157, no. 1, pp. 11–27, Jun. 2006.

- [47] B. E. Conway and W. G. Pell, "Double-layer and pseudocapacitance types of electrochemical capacitors and their applications to the development of hybrid devices," *J. Solid State Electrochem.*, vol. 7, no. 9, pp. 637–644, Sep. 2003.
- [48] A. Razaq, L. Nyholm, M. Sjödin, M. Strømme, and A. Mihranyan, "Paper-Based Energy-Storage Devices Comprising Carbon Fiber-Reinforced Polypyrrole-Cladophora Nanocellulose Composite Electrodes," *Adv. Energy Mater.*, vol. 2, no. 4, pp. 445–454, 2012.
- [49] H. Li, J. Wang, Q. Chu, Z. Wang, F. Zhang, and S. Wang, "Theoretical and experimental specific capacitance of polyaniline in sulfuric acid," *J. Power Sources*, vol. 190, no. 2, pp. 578–586, May 2009.
- [50] L.-Z. Fan and J. Maier, "High-performance polypyrrole electrode materials for redox supercapacitors," *Electrochem. commun.*, vol. 8, no. 6, pp. 937–940, Jun. 2006.
- [51] T. A. Centeno and F. Stoeckli, "The role of textural characteristics and oxygen-containing surface groups in the supercapacitor performances of activated carbons," *Electrochim. Acta*, vol. 52, no. 2, pp. 560–566, Oct. 2006.
- [52] E. Frackowiak, G. Lota, J. Machnikowski, C. Vix-Guterl, and F. Béguin, "Optimisation of supercapacitors using carbons with controlled nanotexture and nitrogen content," *Electrochim. Acta*, vol. 51, no. 11, pp. 2209–2214, Feb. 2006.
- [53] K. Fic, E. Frackowiak, and F. Béguin, "Unusual energy enhancement in carbon-based electrochemical capacitors," *J. Mater. Chem.*, vol. 22, no. 46, p. 24213, Nov. 2012.
- [54] G. Lota and E. Frackowiak, "Striking capacitance of carbon/iodide interface," *Electrochem. commun.*, vol. 11, no. 1, pp. 87–90, Jan. 2009.
- [55] R. . Kalyoncu and H. . J. Taylor, *Kirk-Othmer Encyclopedia of Chemical Technology*, 5th ed. Hoboken: Wiley, 2005, p. 771.
- [56] P. Wallace, "The Band Theory of Graphite," *Phys. Rev.*, vol. 71, no. 9, pp. 622–634, May 1947.
- [57] K. I. Bolotin, K. J. Sikes, Z. Jiang, M. Klima, G. Fudenberg, J. Hone, P. Kim, and H. L. Stormer, "Ultrahigh electron mobility in suspended graphene," *Solid State Commun.*, vol. 146, no. 9–10, pp. 351–355, Jun. 2008.
- [58] A. K. Geim, "Graphene: status and prospects.," *Science*, vol. 324, no. 5934, pp. 1530–4, Jun. 2009.

- [59] A. K. Geim and K. S. Novoselov, "The rise of graphene.," *Nat. Mater.*, vol. 6, no. 3, pp. 183–91, Mar. 2007.
- [60] H.-P. Boehm and E. Stumpp, "No Title," *Carbon N. Y.*, vol. 45, p. 1381, 2007.
- [61] C. Schafhaeutl and J. Prakt., "No Title," *Chem*, vol. 21, no. 129, 1840.
- [62] W. Gao, L. B. Alemany, L. Ci, and P. M. Ajayan, "New insights into the structure and reduction of graphite oxide.," *Nat. Chem.*, vol. 1, no. 5, pp. 403–8, Aug. 2009.
- [63] W. S. Hummers and R. E. Offeman, "Preparation of Graphitic Oxide," *J. Am. Chem. Soc.*, vol. 80, no. 6, p. 1339, Mar. 1958.
- [64] Y. Si and E. T. Samulski, "Synthesis of water soluble graphene.," *Nano Lett.*, vol. 8, no. 6, pp. 1679–82, Jun. 2008.
- [65] B. . Brodie, "On the Atomic Weight of Graphite," *Philos. Trans. R. Scoeity*, vol. 149, p. 249, 1859.
- [66] B. C. Brodie, "XXIII.?Researches on the atomic weight of graphite," *Q. J. Chem. Soc. London*, vol. 12, no. 1, p. 261, Jan. 1860.
- [67] R. R. Nair, P. Blake, A. N. Grigorenko, K. S. Novoselov, T. J. Booth, T. Stauber, N. M. R. Peres, and A. K. Geim, "Fine structure constant defines visual transparency of graphene.," *Science*, vol. 320, no. 5881, p. 1308, Jun. 2008.
- [68] T. W. Ebbesen and P. M. Ajayan, "Large-scale synthesis of carbon nanotubes," *Nature*, vol. 358, no. 6383, pp. 220–222, Jul. 1992.
- [69] S. Frank, "Carbon Nanotube Quantum Resistors," *Science (80-. )*, vol. 280, no. 5370, pp. 1744–1746, Jun. 1998.
- [70] W. Liang, M. Bockrath, D. Bozovic, J. H. Hafner, M. Tinkham, and H. Park, "Fabry - Perot interference in a nanotube electron waveguide.," *Nature*, vol. 411, no. 6838, pp. 665–9, Jun. 2001.
- [71] P. Kim, L. Shi, A. Majumdar, and P. McEuen, "Thermal Transport Measurements of Individual Multiwalled Nanotubes," *Phys. Rev. Lett.*, vol. 87, no. 21, p. 215502, Oct. 2001.
- [72] G. Gao, T. Çagin, and W. A. Goddard, "Energetics, structure, mechanical and vibrational properties of single-walled carbon nanotubes," *Nanotechnology*, vol. 9, no. 3, pp. 184–191, Sep. 1998.

- [73] C. Niu, E. K. Sichel, R. Hoch, D. Moy, and H. Tennent, "High power electrochemical capacitors based on carbon nanotube electrodes," *Appl. Phys. Lett.*, vol. 70, no. 11, p. 1480, Mar. 1997.
- [74] H. Shi, "Activated carbons and double layer capacitance," *Electrochim. Acta*, vol. 41, no. 10, pp. 1633–1639, Jun. 1996.
- [75] J. Gamby, P. Taberna, P. Simon, J. Fauvarque, and M. Chesneau, "Studies and characterisations of various activated carbons used for carbon/carbon supercapacitors," *J. Power Sources*, vol. 101, no. 1, pp. 109–116, Oct. 2001.
- [76] Y. Kim, Y. Horie, S. Ozaki, Y. Matsuzawa, H. Suezaki, C. Kim, N. Miyashita, and M. Endo, "Correlation between the pore and solvated ion size on capacitance uptake of PVDC-based carbons," *Carbon N. Y.*, vol. 42, no. 8–9, pp. 1491–1500, Jan. 2004.
- [77] K. Jurewicz, C. Vix-Guterl, E. Frackowiak, S. Saadallah, M. Reda, J. Parmentier, J. Patarin, and F. Béguin, "Capacitance properties of ordered porous carbon materials prepared by a templating procedure," *J. Phys. Chem. Solids*, vol. 65, no. 2–3, pp. 287–293, Mar. 2004.
- [78] J. A. Fernández, T. Morishita, M. Toyoda, M. Inagaki, F. Stoeckli, and T. A. Centeno, "Performance of mesoporous carbons derived from poly(vinyl alcohol) in electrochemical capacitors," *J. Power Sources*, vol. 175, no. 1, pp. 675–679, Jan. 2008.
- [79] N.-L. Wu, "Nanocrystalline oxide supercapacitors," *Mater. Chem. Phys.*, vol. 75, no. 1–3, pp. 6–11, Apr. 2002.
- [80] T. Brousse, M. Toupin, R. Dugas, L. Athouël, O. Crosnier, and D. Bélanger, "Crystalline MnO<sub>2</sub> as Possible Alternatives to Amorphous Compounds in Electrochemical Supercapacitors," *J. Electrochem. Soc.*, vol. 153, no. 12, p. A2171, Dec. 2006.
- [81] A. Rudge, J. Davey, I. Raistrick, S. Gottesfeld, and J. P. Ferraris, "Conducting polymers as active materials in electrochemical capacitors," *J. Power Sources*, vol. 47, no. 1–2, pp. 89–107, Jan. 1994.
- [82] S. Iijima, "Helical microtubules of graphitic carbon," *Nature*, vol. 354, no. 6348, pp. 56–58, Nov. 1991.
- [83] A. Allaoui, "Mechanical and electrical properties of a MWNT/epoxy composite," *Compos. Sci. Technol.*, vol. 62, no. 15, pp. 1993–1998, Nov. 2002.



- [84] J.-P. Salvetat, J.-M. Bonard, N. H. Thomson, A. J. Kulik, L. Forró, W. Benoit, and L. Zuppiroli, “Mechanical properties of carbon nanotubes,” *Appl. Phys. A Mater. Sci. Process.*, vol. 69, no. 3, pp. 255–260, Sep. 1999.
- [85] C. Portet, G. Yushin, and Y. Gogotsi, “Electrochemical performance of carbon onions, nanodiamonds, carbon black and multiwalled nanotubes in electrical double layer capacitors,” *Carbon N. Y.*, vol. 45, no. 13, pp. 2511–2518, Nov. 2007.
- [86] Y. C. Sui, D. R. Acosta, J. A. González-León, A. Bermúdez, J. Feuchtwanger, B. Z. Cui, J. O. Flores, and J. M. Saniger, “Structure, Thermal Stability, and Deformation of Multibranching Carbon Nanotubes Synthesized by CVD in the AAO Template,” *J. Phys. Chem. B*, vol. 105, no. 8, pp. 1523–1527, Mar. 2001.
- [87] L. Dai, D. W. Chang, J.-B. Baek, and W. Lu, “Carbon nanomaterials for advanced energy conversion and storage,” *Small*, vol. 8, no. 8, pp. 1130–66, Apr. 2012.
- [88] Y. He, W. Chen, C. Gao, J. Zhou, X. Li, and E. Xie, “An overview of carbon materials for flexible electrochemical capacitors,” *Nanoscale*, vol. 5, no. 19, pp. 8799–820, Oct. 2013.
- [89] S. Bose, T. Kuila, A. K. Mishra, N. H. Kim, and J. H. Lee, “Dual role of glycine as a chemical functionalizer and a reducing agent in the preparation of graphene: an environmentally friendly method,” *J. Mater. Chem.*, vol. 22, no. 19, p. 9696, Apr. 2012.
- [90] H. Jiang, P. S. Lee, and C. Li, “3D carbon based nanostructures for advanced supercapacitors,” *Energy Environ. Sci.*, vol. 6, no. 1, p. 41, Dec. 2013.
- [91] S. Park, M. Vosguerichian, and Z. Bao, “A review of fabrication and applications of carbon nanotube film-based flexible electronics,” *Nanoscale*, vol. 5, no. 5, pp. 1727–52, Mar. 2013.
- [92] Y. J. Kang, S.-J. Chun, S.-S. Lee, B.-Y. Kim, J. H. Kim, H. Chung, S.-Y. Lee, and W. Kim, “All-solid-state flexible supercapacitors fabricated with bacterial nanocellulose papers, carbon nanotubes, and triblock-copolymer ion gels,” *ACS Nano*, vol. 6, no. 7, pp. 6400–6, Jul. 2012.
- [93] L. Hu, W. Chen, X. Xie, N. Liu, Y. Yang, H. Wu, Y. Yao, M. Pasta, H. N. Alshareef, and Y. Cui, “Symmetrical MnO<sub>2</sub>-carbon nanotube-textile nanostructures for wearable pseudocapacitors with high mass loading,” *ACS Nano*, vol. 5, no. 11, pp. 8904–13, Nov. 2011.
- [94] G. Yu, X. Xie, L. Pan, Z. Bao, and Y. Cui, “Hybrid nanostructured materials for high-performance electrochemical capacitors,” *Nano Energy*, vol. 2, no. 2, pp. 213–234, Mar. 2013.

- [95] G. Nyström, A. Razaq, M. Strømme, L. Nyholm, and A. Mihranyan, “Ultrafast All-Polymer Paper-Based Batteries,” *Nano Lett.*, vol. 9, no. 10, pp. 3635–3639, Sep. 2009.
- [96] C. Meng, C. Liu, L. Chen, C. Hu, and S. Fan, “Highly Flexible and All-Solid-State Paperlike Polymer Supercapacitors,” *Nano Lett.*, vol. 10, no. 10, pp. 4025–4031, Sep. 2010.
- [97] Y. Zhu, S. Murali, M. D. Stoller, K. J. Ganesh, W. Cai, P. J. Ferreira, A. Pirkle, R. M. Wallace, K. A. Cychosz, M. Thommes, D. Su, E. A. Stach, and R. S. Ruoff, “Carbon-Based Supercapacitors Produced by Activation of Graphene,” *Sci.*, vol. 332, no. 6037, pp. 1537–1541, Jun. 2011.
- [98] T. Chen and L. Dai, “Flexible supercapacitors based on carbon nanomaterials,” *J. Mater. Chem. A*, Apr. 2014.
- [99] Y. Cheng, S. Lu, H. Zhang, C. V Varanasi, and J. Liu, “Synergistic effects from graphene and carbon nanotubes enable flexible and robust electrodes for high-performance supercapacitors,” *Nano Lett.*, vol. 12, no. 8, pp. 4206–11, Aug. 2012.
- [100] L. Bao and X. Li, “Towards textile energy storage from cotton T-shirts,” *Adv. Mater.*, vol. 24, no. 24, pp. 3246–52, Jun. 2012.
- [101] L. Hu, M. Pasta, F. La Mantia, L. Cui, S. Jeong, H. D. Deshazer, J. W. Choi, S. M. Han, and Y. Cui, “Stretchable, porous, and conductive energy textiles,” *Nano Lett.*, vol. 10, no. 2, pp. 708–14, Feb. 2010.
- [102] L. Hu and Y. Cui, “Energy and environmental nanotechnology in conductive paper and textiles,” *Energy Environ. Sci.*, vol. 5, no. 4, p. 6423, Mar. 2012.
- [103] R. E. Lee, *Phycology*. Cambridge University Press, 1999, p. 614.
- [104] R. Ek, C. Gustafsson, A. Nutt, T. Iversen, and C. Nyström, “Cellulose powder from *Cladophora* sp. algae,” *J. Mol. Recognit.*, vol. 11, no. 1–6, pp. 263–265, 1998.
- [105] Z. Gui, H. Zhu, E. Gillette, X. Han, G. W. Rubloff, L. Hu, and S. B. Lee, “Natural cellulose fiber as substrate for supercapacitor,” *ACS Nano*, vol. 7, no. 7, pp. 6037–46, Jul. 2013.
- [106] Z. Weng, Y. Su, D.-W. Wang, F. Li, J. Du, and H.-M. Cheng, “Graphene-Cellulose Paper Flexible Supercapacitors,” *Adv. Energy Mater.*, vol. 1, no. 5, pp. 917–922, Oct. 2011.

- [107] T. T and H. C, “Electrochemical Applications of Room-Temperature Ionic Liquids,” *Electrochem. Soc. Interface*, vol. 16, no. 1, pp. 42–49, 2007.
- [108] J. Zhang and X. S. Zhao, “On the configuration of supercapacitors for maximizing electrochemical performance.,” *ChemSusChem*, vol. 5, no. 5, pp. 818–41, May 2012.
- [109] G. Nyström, A. Mihranyan, A. Razaq, T. Lindström, L. Nyholm, and M. Strømme, “A Nanocellulose Polypyrrole Composite Based on Microfibrillated Cellulose from Wood,” *J. Phys. Chem. B*, vol. 114, no. 12, pp. 4178–4182, Mar. 2010.
- [110] A. N. Aphale, A. Chattopadhyay, K. Mahakalkar, and P. K. Patra, “Synthesis and Electrochemical Analysis of Algae Cellulose-Polypyrrole-Graphene Nanocomposite for Supercapacitor Electrode,” *J. Nanosci. Nanotechnol.*, vol. 15, pp. 6225–6229, 2015.
- [111] A. Bhattacharya, J. Cheng, S. Bhosale, A. Aphale, I. Macwan, P. K. Patra, and I. Mukerji, “UV Resonance Raman Characterization of Diphenylalanine-Graphene Nanotubes,” *Spectroscopy*, vol. 27, no. 11, pp. 40–47, Nov. 2012.
- [112] D. R. Dreyer, S. Park, C. W. Bielawski, and R. S. Ruoff, “The chemistry of graphene oxide.,” *Chem. Soc. Rev.*, vol. 39, no. 1, pp. 228–40, Jan. 2010.
- [113] J. I. Paredes, S. Villar-Rodil, A. Martínez-Alonso, and J. M. D. Tascón, “Graphene Oxide Dispersions in Organic Solvents,” *Langmuir*, vol. 24, no. 19, pp. 10560–10564, Aug. 2008.
- [114] H. A. Becerril, J. Mao, Z. Liu, R. M. Stoltenberg, Z. Bao, and Y. Chen, “Evaluation of Solution-Processed Reduced Graphene Oxide Films as Transparent Conductors,” *ACS Nano*, vol. 2, no. 3, pp. 463–470, Feb. 2008.
- [115] S. Li, A. N. Aphale, I. G. Macwan, P. K. Patra, W. G. Gonzalez, J. Miksovská, and R. M. Leblanc, “Graphene oxide as a quencher for fluorescent assay of amino acids, peptides, and proteins.,” *ACS Appl. Mater. Interfaces*, vol. 4, no. 12, pp. 7069–75, Dec. 2012.
- [116] A. Das, B. Chakraborty, and A. K. Sood, “Raman spectroscopy of graphene on different substrates and influence of defects,” *Bull. Mater. Sci.*, vol. 31, no. 3, pp. 579–584, 2008.
- [117] F. Jiang, T. Zhou, S. Tan, Y. Zhu, Y. Liu, and D. Yuan, “Porous Polypyrrole Prepared by Using Nanoscale Calcium Carbonate as a Core for Supercapacitance Materials,” *Int. J. Electrochem. Sci.*, vol. 4, pp. 1541–1547, 2009.

- [118] A. Mirmohseni, W. E. Price, G. G. Wallace, and H. Zhao, "Adaptive Membrane Systems Based on Conductive Electroactive Polymers," *J. Intell. Mater. Syst. Struct.*, vol. 4, no. 1, pp. 43–49, Jan. 1993.
- [119] R. Ansari, "In-situ cyclic voltammetry and cyclic resistometry analyses of conducting electroactive polymer membranes.," *Intern. J. ChemTech Res.*, vol. 14, pp. 1398–1402, 2009.
- [120] L. Mai, H. Li, Y. Zhao, L. Xu, X. Xu, Y. Luo, Z. Zhang, W. Ke, C. Niu, and Q. Zhang, "Fast Ionic Diffusion-Enabled Nanoflake Electrode by Spontaneous Electrochemical Pre-Intercalation for High-Performance Supercapacitor," *Sci. Rep.*, vol. 3, Apr. 2013.
- [121] Z. Bo, Z. Wen, H. Kim, G. Lu, K. Yu, and J. Chen, "One-step fabrication and capacitive behavior of electrochemical double layer capacitor electrodes using vertically-oriented graphene directly grown on metal," *Carbon N. Y.*, vol. 50, no. 12, pp. 4379–4387, Oct. 2012.
- [122] A. Ziabicki, *Fundamentals of fibre formation : the science of fibre spinning and drawing*. London ;,New York: Wiley, 1976.
- [123] P. Katta, M. Alessandro, R. D. Ramsier, and G. G. Chase, "Continuous Electrospinning of Aligned Polymer Nanofibers onto a Wire Drum Collector," *Nano Lett.*, vol. 4, no. 11, pp. 2215–2218, Sep. 2004.
- [124] M. Lewin, *Handbook of Fiber Chemistry*, Third. New York: CRC, 2006, pp. 205–218.
- [125] G. E. Hagler, "Qualitative prediction of the effects of changes in spinning conditions on spun fiber orientation," *Polym. Eng. Sci.*, vol. 21, no. 3, pp. 121–123, 1981.
- [126] J. Drew, "Battery-Free Power Backup System Uses Supercapacitors to Prevent Data Loss in RAID Systems," *LT Journal of Analog Innovation*, pp. 31–35, 2010.
- [127] Z. G. Cambaz, G. Yushin, S. Osswald, V. Mochalin, and Y. Gogotsi, "Noncatalytic synthesis of carbon nanotubes, graphene and graphite on SiC," *Carbon N. Y.*, vol. 46, no. 6, pp. 841–849, May 2008.